Low Dielectric Constant Insulators and Gold Metallization for GHz Multi-Chip Modules

Part 2.

DARPA BAA#90-09, Part II
Contract: N00014-91-J-4008

Annual Performance Report
July, 1993

Principal Investigators:

Paul Kohl and Sue Ann Bidstrup
School of Chemical Engineering

David Hertling
School of Electrical Engineering

Georgia Institute of Technology
Atlanta, GA 30332-0100

1. Overview

The goal of this program is to investigate new dielectrics, metals and processes for the fabrication of multi-chip modules which hold the promise of exceptional electrical performance in the GHz region in addition to high yield and high reliability. The low dielectric constant insulators are being evaluated through the fabrication of in-situ test structures using noble metals. In the course of doing this evaluation, a simple process for gold or silver MCMs has been investigated.

A processing scheme using noble metals (gold and silver) as the interconnection metallization in the module has been developed and is being characterized. The noble metal process has fewer process steps than the equivalent copper process and is potentially lower cost, particularly when high reliability is important. It has been observed that silver has an advantage in that it maintains its bulk conductivity during high temperature processing and has low residual stress. In addition, a unique adhesion material has been investigated and is currently being applied by n-Chip. This adhesion material would result in a significant cost reduction in the manufacture of copper or gold MCMs. The silver metallization technology and SiO_2 characterization is also being conducted with n-Chip.

A second generation test module has been fabricated to provide test structures to evaluate new polymers and metals for multi-chip module applications. About half of the real estate is devoted to microwave structures designed at the Mayo clinic called "The High Frequency Passive Structure Coupon". The process has two ground layers and two signal layers, and incorporates both microstrip and stripline waveguides, with characteristic impedance of 50 ohms, facilitating measurement with standard test equipment well up into the gigahertz regime. The emphasis for these structures is on evaluating high frequency electrical performance of actual MCM devices (waveguides).

A short list of organic and inorganic materials have been selected for evaluation as interlevel dielectrics with the noble metal interconnects. In-situ test structures are being fabricated to determine the electrical, mechanical and chemical properties of the dielectrics. Novel approaches to low dielectric constant insulators are being investigated in addition to the evaluation of existing

materials. New techniques are being evaluated for rapid curing of polymer dielectrics.

Selection of thin film dielectrics is a key element in the performance and long-term reliability of GHz multichip modules. The overall performance depends on the ease of processing, chemical structure, electrical behavior and mechanical properties. Crucial characteristics which must be considered in the selection of materials to be used as interlevel dielectrics include: dielectric properties; moisture absorption; coefficient of thermal expansion; modulus; residual stress; adhesion; processing temperature; thermal stability; and thermal conductivity. The short list of polymers currently being investigated for use in GHz frequency MCMs include:

DuPont PI2545 (PMDA-ODA)
DuPont PI2566 (Fluorinated)
DuPont PI2611 (Low Stress)
Amoco Ultadel 7501 (Photosensitive)
Ciba-Geigy 400 Series (Pre-imidized and Photosensitive)
Allied-Maxdem polyquinolines
Dow Chemical benzocyclobutenes

A number of inorganic materials have also been explored for interlevel dielectric applications, including:

Plasma Enhanced CVD Silicon Dioxide
Spin-on Glasses
Porous Silica

Studies are underway to investigate the improvement in silicon dioxide performance through variations in deposition conditions. The effect of the measurement frequency on the dielectric properties of silicon dioxide is also being explored. The use of spin-on glasses and porous silica as interlevel dielectrics has been explored; it was determined that processing problems resulted in limited use in this application.

In order to compare the performance properties of the various dielectric materials, in-situ characterization techniques are required. Thermal cure history,

fabrication environment and type of substrate upon which the pre-polymer is cast all can have a significant effect on the final film properties. Therefore, a polymer film cured on a particular surface may have significantly different properties than a film of the same material cured free of the substrate. In order that the characterization test results actually reflect the behavior of the polymer in a performance environment, it is necessary to measure the critical film properties directly on the substrate.

A number of methods are being used or developed for characterizing film properties directly on a silicon or metallized substrate. The in-plane modulus is characterized using micro-machined low deflection sites or microfabricated vibrating polymer strings. The residual stress and in-plane coefficient of thermal expansion are measured using a Flexus Wafer Curvature Apparatus. The film thickness, refractive indices and degree of orientation are obtained using a Metricon Prism Coupler.

In applications requiring multilayer coatings, polymer properties normal to the plane are as crucial to the performance of the coating as polymer properties in the plane. Each of the characterization techniques mentioned above are restricted to the characterization of in-plane properties. The spin coat processing of polymer films may lead to molecules which are oriented in the plane of the film; this orientation will cause the electrical, mechanical and thermal properties in the plane of the film to be different from those properties through the plane of the film. Currently, there is no test method for measuring mechanical and thermal properties normal to the plane of the film. In this study the microfabricated electrodes will be used to determine small changes in film thickness that result when the temperature or pressure in the film is varied. From these measurements, we can directly determine the modulus and the coefficient of thermal expansion normal to the plane of the film.

In summary, a second generation noble metal-insulator test structure has been fabricated to evaluate the performance of various interconnection metal and dielectrics. A series of promising organic and inorganic dielectrics have been selected for evaluation for use in GHz multi-chip modules. A series of in-situ characterization techniques have been developed for measuring electrical, mechanical and thermal properties of the interlevel dielectrics. The effect of the chemical system and processing variations on the performance properties of thin film dielectrics is currently being explored. Processing variations include the

spin speed, film thickness, reaction temperature and degree of molecular orientation.

Milestones:

Date Proposed	Date Completed	Technical Objective
8/1991	9/1991	Initiate Program.
9/1991	9/1991	Training of graduate and undergraduate students on specific processing and testing equipment.
10/1991	10/1991	Selection of "Long List" of low dielectric constant materials and structures.
12/1991	11/1991	Fixtures for HP8510 completed.
12/1991	12/1991	Completion of process log for test structure processing to evaluate low dielectric constant materials and processes.
1/1992	12/1991	Design of in-situ stress and mechanical property testing.
1/1992	12/1991	Fabrication of first generation test structures for characterization.
3/1992	2/1992	Identification of layer to layer adhesion test.
4/1992	1/1991	First Georgia Tech electrical characterization of microstrips at >1 GHz.
7/1992	11/1992	Preliminary design of second test structure in collaboration with outside institution of DARPA's choosing.

8/1992	11/1992	Preliminary evaluation of stress and high frequency electrical properties of low dielectric constant material.
10/1992	11/1992	Selected short list of low dielectric constant materials and processes.
11/1992	3/1992	Design of experiments for moisture uptake.
1/1993	1/1993	Evaluation of adhesive properties and development of processing techniques to improve adhesion.
2/1993	2/1993	Preliminary evaluation of gold vs. copper completed.
3/1993	2/1992	Lithography masks of second test structure completed.
9/1993	6/1993	Models of second test structure completed.
11/1993	partial	Evaluation of stress, adhesion and high frequency electrical properties at ambient conditions.
3/1994	partial	In-depth high frequency characterization of chemical structure vs. equivalent circuit.
7/1994		Effect of moisture and temperature cycling on adhesion and high frequency electrical properties.
8/1994		Documentation completed.

2. Second Generation Test Module

The purpose of this mask set is to provide test structures to evaluate new polymers and metals for multi-chip module (MCM) applications. About half of the real estate is devoted to microwave structures designed at the Mayo clinic called "The High Frequency Passive Structure Coupon". The process has two ground layers and two signal layers and incorporates both microstrip and stripline waveguides, with characteristic impedance of 50 ohms, facilitating measurement with standard test equipment well up into the gigahertz regime. The emphasis for these structures is on evaluating high frequency electrical performance of actual MCM devices (waveguides). Five basic types of measurements will be made by the Mayo clinic: DC resistance, capacitance, S-parameter, time domain reflectometry (TDR), and time domain transmission (TDT).

DC resistance measurements will be made with a four point Kelvin meter. Probes that are made specifically for use with Kelvin meters will be used.

S-parameter measurements will be made with an HP 8510 vector network analyzer. Single line structures will be measured from 45MHz to 18GHz and dual line measurements from 45MHz to 9GHz. Transmission, reflection, and crosstalk measurements will be plotted individually at time of measurement over the entire frequency band.

Time Domain Refectometry measurements will have a similar setup as those of the S-parameters. The actual plots of the TDR measurements will consist of a near end open, near end short, far end open, and far end teminated signal traces.

Time Domain Transmission, which is similar to TDR, will be used on the crosstalk structures. This consists of injecting a TDR pulse on one line, while looking at all other signal ports with an oscilloscope. Plots will have time as the horizontal scale and voltage as the vertical scale.

To characterize a single transmission line, there are three lengths of single lines on each of the two signal routing layers: 4.0 cm, 2.0 cm, and 1.0 cm (structures #1-#10 in the structures list below). These are simple, straight transmission lines with no bends or vias. DC resistance, S-parameter and TDR measurements will be made on these structures. In addition, the 4.0 cm line is duplicated in three locations across the coupon to check for variation across the sample.

Structures #23 - #40 investigate intralevel crosstalk by placing segments of parallel transmission lines in proximity to each other. Three different lengths and three different separations are used. DC resistance, S-parameter, and TDR measurements will be made on these structures.

There are a total of six lines (#11 - #16) for use in determining the electrical characteristics of bends, one set of three for each routing layer. Each set of three lines will contain exactly four right angle bends per line. DC resistance, S-parameter and TDR measurements will be made on these.

The following is a table listing the devices included in the Mayo design.

The Mayo Clinic's "High Frequency Passive Test Structures"

#	Structure Name	Length(cm)	Description
1)	SL1-1	1	Straight Microstrip
2)	Sl1-2	1	Straight Stripline
3)	SL2-1	2	Straight Microstrip
4)	SL2-2	2	Straight Stripline
5)	SL4-1A	4	Straight Microstrip
6)	SL4-1B	4	Straight Microstrip
7)	SL4-1C	4	Straight Microstrip
8)	SL4-2A	4	Straight Stripline
9)	SL4-2B	4	Straight Stripline
10)	SL4-2C	4	Straight Stripline
11)	BD1-1	4	Microstrip bends, 0.9cm center segment

12)	BD1-2	4	Stripline bends, 0.9cm center segment
13)	BD2-1	4	Microstrip bends, 1.8cm center segment
14)	BD2-2	4	Stripline bends, 1.8cm center segment
15)	BD4-1	4	Microstrip bends, 3.6cm center segment
16)	BD4-2	4	Stripline bends, 3.6cm center segment
17)	VA1-1	4	Microstrip with vias, 0.9cm center segment
18)	VA1-2	4	Stripline with vias, 0.9cm center segment
19)	VA2-1	4	Microstrip with vias, 1.8cm center segment
20)	VA2-2	4	Stripline with vias, 1.8cm center segment
21)	VA4-1	4	Microstrip with vias, 3.6cm center segment
22)	VA4-2	4	Stripline with vias, 3.6cm center segment
23)	XT1-10-1	4	Microstrip crosstalk, 0.9cm center, 50mm separation
24)	XT1-10-2	4	Stripline crosstalk, 0.9cm center, 50mm separation
25)	XT1-20-1	4	Microstrip crosstalk, 0.9cm center, 100mmseparation
26)	XT1-20-2	4	Stripline crosstalk, 0.9cm center, 100mm separation
27)	XT1-40-1	4	Microstrip crosstalk, 0.9cm center, 200mm separation
28)	XT1-40-2	4	Stripline crosstalk, 0.9cm center, 200mm separation
29)	XT2-10-1	4	Microstrip crosstalk, 1.8cm center, 50mm separation
30)	XT2-10-2	4	Stripline crosstalk, 1.8cm center, 50mm separation
31)	XT2-20-1	4	Microstrip crosstalk, 1.8cm center, 100mm separation
32)	XT2-20-2	4	Stripline crosstalk, 1.8cm center, 100mm separation
33)	XT2-40-1	4	Microstrip crosstalk, 1.8cm center, 200mm separation
34)	XT2-40-2	4	Stripline crosstalk, 1.8cm center, 200mm separation
35)	XT4-10-1	4	Microstrip crosstalk, 3.6cm center, 50mm separation
36)	XT4-10-2	4	Stripline crosstalk, 3.6cm center, 50mm separation
37)	XT4-20-1	4	Microstrip crosstalk, 3.6cm center, 100mm separation
38)	XT4-20-2	4	Stripline crosstalk, 3.6cm center, 100mm separation
39)	XT4-40-1	4	Microstrip crosstalk, 3.6cm center, 200mm separation
40)	XT4-40-2	4	Stripline crosstalk, 3.6cm center, 200mm separation
41)	R1	0.06	Integral 50 ohm resistor to ground
42)	R2	0.06	Soldered 50 ohm resistor to ground
43)	R3	0.06	Bonded 50 ohm resistor to ground
44)	R4	0.06	Integral 50 ohm resistor to ground
45)	C12	0	Capacitor between layers 1 and 2
46)	C23	0	Capacitor between layers 2 and 3
47)	C34	0	Capacitor between layers 3 and 4

48)	V1	0	Verificaton sites, open pads
49)	V2	0	Verificaton sites, shorts, same probe
50)	V3	0	Verificaton sites, shorts to ground
51)	V4	0.1	Microstrip shorts between probes
52)	V5	0.1	Stripline shorts between probes

The remainder of the real estate is used by structures designed at Georgia Tech in order to evaluate materials properties of the metals and polymers used. The Georgia Tech structures include:

1) Interdigitated electrodes - These are the comb capacitors described elsewhere. These along with the parallel plate capacitors can be used to determine permittivity, loss and modulus.

2) Parallel plate capacitors - These structures are used to determine the low frequency electrical properties of interlevel dielectrics.

3) Moisture uptake structures - These structures are combs similar to the interdigitated electrodes but have only one comb instead of two. They will be used to look at the effect of moisture absorption.

4) Interlevel shorts - These are serpentine patterns of overlying metal to investigate interlevel shorts. They are 10mm lines and spaces covering an area of 0.4cm by 0.4cm. There is one for level four to level three and one for level 3 to level 2.

5) End gap microstrip resonators - These are used to determine permittivity and loss of the waveguides. By looking at nulls in the coupled energy versus frequency accurate determination of the parameters is possible

6) "T" shaped microstrip resonators - These are very similar to the endgap resonators but incorporate a different waveguide structure allowing for a second type of structure for determination of the parameters.

3. Metallization

3.1 Evaluation of Silver

Purpose

The purpose of this investigation was to evaluate silver as a possible alternative to standard conductors in MCM fabrication. The electroplated and sputtered silver films were evaluated in terms of conductivity, residual stress, and purity.

Conductivity

Two plating solutions were originally chosen for the conductivity evaluation of the electroplated silver. A proprietary silver cyanide plating solution from Technic Inc. was purchased which contained two different additives to brighten the plated films. A $KAg(CN)_2$ solution was also prepared that was identical to the proprietary solution minus the additives. The electroplated films were deposited at room temperature at a current density of 3.7 mA/cm^2, while the sputtered silver was deposited using a DC magnetron sputtering at a deposition rate of 5.6 Å/s. In both cases the conductivities were measured on two different four-point probe instruments, one of which was capable of achieving 4 K.

The effect of high-temperature processing on the conductivity of the electroplated and sputtered silver was also evaluated. In turn, the effects of depositing an inorganic dielectric (SiO_2), a dry polymer (BCB), and a wet polymer (PI 2545) on the silver films were observed at both normal and extreme processing conditions. The normal processing conditions were to mimic the actual application of the dielectric, while the extreme processing conditions were to simulate the repeated thermal punishment of subsequent dielectric layer depositions.

The additive-free $KAg(CN)_2$ solution consistently produced silver films whose conductivity was 95% of the bulk value for silver. The proprietary solution delivered films whose conductivity was only 77% of bulk, presumably due to the deleterious incorporation of the additives into the film during the electroplating. As such, the proprietary solution was discarded in favor of the

additive-free solution, and no further evaluation of the proprietary solution took place. The conductivity of the sputtered films was consistently measured at 84% of the bulk value.

The results of the dielectric processing conditions for the electroplated silver can be seen in Tabless 3.1-1 and 3.1-2. In the case of SiO_2 and BCB, the conductivity of electroplated silver consistently increased to 100% of the bulk value in both the normal and extreme cases. Initially for the third dielectric, the PI 2545 polyimide, the conductivity of the electroplated silver was found to decrease to 75% of the bulk value in both cases. As the PI 2545 was the only wet dielectric to be investigated, this decrease in the conductivity was at first attributed to the water in the polymer. But after further analysis, it was determined that the method used to remove the cured polymer from the silver film was responsible for the decrease in the conductivity. An improved method of film removal was employed, and the conductivity of the electroplated silver under the PI 2545 film was also found to increase to 100% of bulk.

The corresponding results for the sputtered silver can be seen in Tables 3.1-3 and 3.1-4. In the case of SiO_2 and BCB, and PI 2545 the conductivity of sputtered silver consistently increased to only 94% of the

resistivity before	dielectric process	resistivity after
1.66×10^{-6} Ω•cm	SiO_2 - 250 °C	1.57×10^{-6} Ω•cm
1.65×10^{-6} Ω•cm	BCB - 290 °C, 13 sec	1.57×10^{-6} Ω•cm
1.67×10^{-6} Ω•cm	PI 2545 - 350 °C, 1 hr	1.58×10^{-6} Ω•cm

Table 3.1-1. Normal processing conditions - electroplated.

resistivity before	dielectric process	resistivity after
1.62×10^{-6} Ω•cm	SiO_2 - 350 °C	1.57×10^{-6} Ω•cm
1.61×10^{-6} Ω•cm	BCB - 250 °C, 4 hours	1.56×10^{-6} Ω•cm
1.60×10^{-6} Ω•cm	PI 2545 - 350 °C, 4 hours	1.57×10^{-6} Ω•cm

Table 3.1-2 Extreme processing conditions - electroplated.

resistivity before	dielectric process	resistivity after
1.90×10^{-6} Ω•cm	SiO_2 - 250 °C	1.78×10^{-6} Ω•cm
1.92×10^{-6} Ω•cm	BCB - 290 °C, 13 sec	1.69×10^{-6} Ω•cm
1.88×10^{-6} Ω•cm	PI 2545 - 350 °C, 1 hr	1.71×10^{-6} Ω•cm

Table 3.1-3. Normal processing conditions - sputtered.

resistivity before	dielectric process	resistivity after
1.91×10^{-6} Ω•cm	SiO_2 - 350 °C	1.72×10^{-6} Ω•cm
1.90×10^{-6} Ω•cm	BCB - 250 °C, 4 hours	1.73×10^{-6} Ω•cm
1.93×10^{-6} Ω•cm	PI 2545 - 350 °C, 4 hours	1.69×10^{-6} Ω•cm

Table 3.1-4. Extreme processing conditions - sputtered.

bulk value in both the normal and extreme cases. These conductivities were higher than the unprocessed values, yet were significantly lower than the corresponding electroplated values.

Further information regarding this temperature-conductivity relationship can be seen in Figures 3.1-1 and 3.1-2. Two points are worth mentioning. First of all, the higher temperature clearly produced a quicker effect upon the conductivity of the films. But ultimately there was no

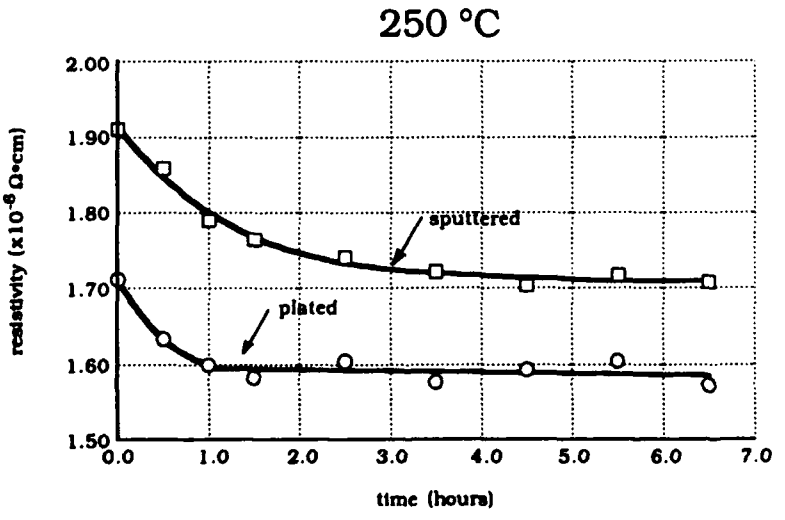

Figure 3.1-1. Resistivity versus time for Ag film at 250 °C.

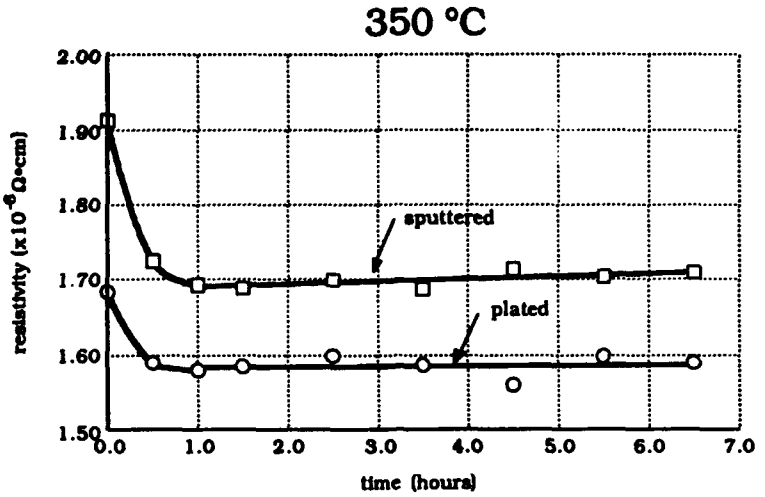

Figure 3.1-2. Resistivity versus time for Ag film at 350 °C.

difference between the treatment at the two temperatures, as given enough time the final conductivity of the films after the 250 °C treatment was identical to the conductivity after the 350 °C treatment. Second of all, it was not possible to push the sputtered silver to bulk conductivity. For both the 250 °C and 350 °C heating cycles, the sputtered silver reached a plateau at a resistivity of 1.70×10^{-6} Ω•cm. In comparison, the electroplated silver went almost immediately to bulk.

Residual Stress

A 2 μm silver film was electroplated on top of a silicon substrate and the composite was subjected to three thermal cycles. The temperature was ramped from room temperature to 350 °C and back at a rate of 3 °C/min. This three step program was designed to mimic one application cure cycle, followed by two more heating cycles simulating the curing of two additional dielectric layers. All three cure cycles took place in a nitrogen atmosphere. An identical method was employed for a 2 μm sputtered film.

The residual stress versus temperature results for the sputtered film can be seen in Figure 3.1-3, and the residual stress versus temperature results for the electroplated film can be seen in Figure 3.1-4. The residual stress of the freshly electroplated silver was measured to be 27 MPa, while the residual stress of the thermally processed electroplated silver was measured to be 72 MPa. The residual stress of the freshly sputtered silver was measured to be 100 MPa, while

the residual stress of the thermally processed sputtered silver was measured to be 220 MPa.

Both the residual stress versus temperature curves for the electroplated and sputtered films followed the general behavior seen for films of this type. As the composite was heated, the slope followed the one expected from the CTE mismatch between the silver and silicon. The elastic limit of the composite was reached between 150-250 °C, above which plastic deformation in the metal film continually mitigated the compressive stress in

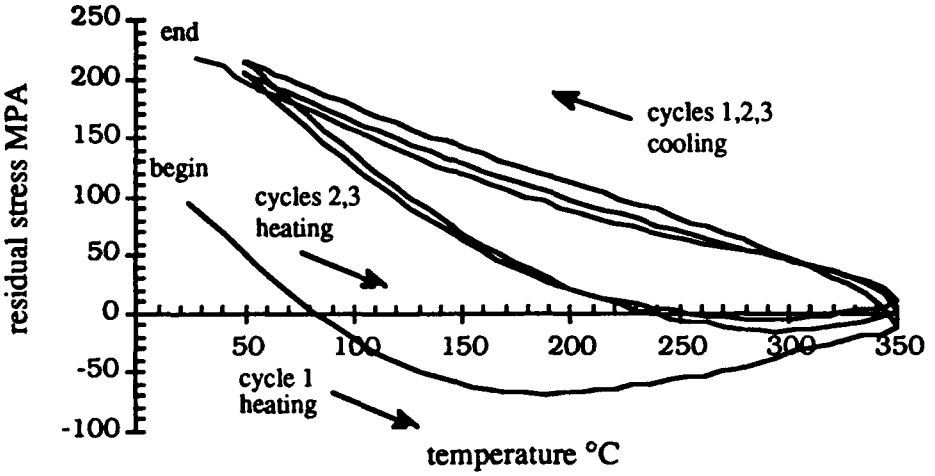

Figure 3.1-3. Residual stress versus temperature for sputtered Ag film.

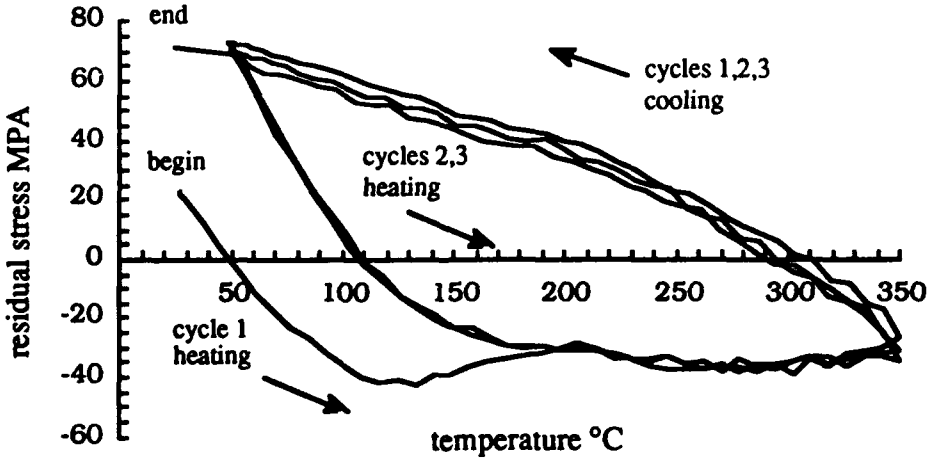

Figure 3.1-4. Residual stress versus temperature for electroplated Ag film.

the composite as the temperature increased. As the composite was cooled, a brief elastic response was then followed by another plastic deformation period, as the stress again exceeded the elastic limit of the composite. The second and third heating cycles behaved precisely as the first, except the curve had been pushed permanently to the right by the vacancy consumption, grain growth, and recrystallization that was unique to the first cycle. The disparity between the final stress magnitudes for the sputtered and electroplated films, as well as the noticably different shapes of the overall stress curves, are currently being investigated.

Purity

The conductivity of two silver samples was measured as the temperature was lowered from room temperature to approximately 16 K. One sample was thermally processed at 200 °C for an hour, while the other received no treatment after being electroplated. The high temperature conductivity behavior of the silver is dominated by electron-phonon scattering. Since the phonon population is proportional to temperature, the conductivity of the silver will be linear with temperature until the phonon population is sufficiently small for the effects of impurities to become apparent. The temperature at which the linear dependence ends is the point that the temperature-independent effects of the impurities take over. The lower the temperature at which this happens, the purer the film.

The results of this evaluation for the electroplated silver can be seen in Figure 3.1-5. The purity of the electroplated silver was excellent, as the linear temperature dependence for the unprocessed sample was maintained until approximately 40 K. The processed sample displayed the linear temperature dependence until approximately 20 K. As seen earlier during the dielectric deposition experiments, heat treatments apparently push any impurities away from the grain boundaries of the silver film, resulting in an improved conductivity at room temperature as well as delaying the onset of impurity-controlled conductivity behavior at low temperature. A similar evaluation for the sputtered silver is currently underway, and this evaluation will mimic the electroplated analysis in every regard.

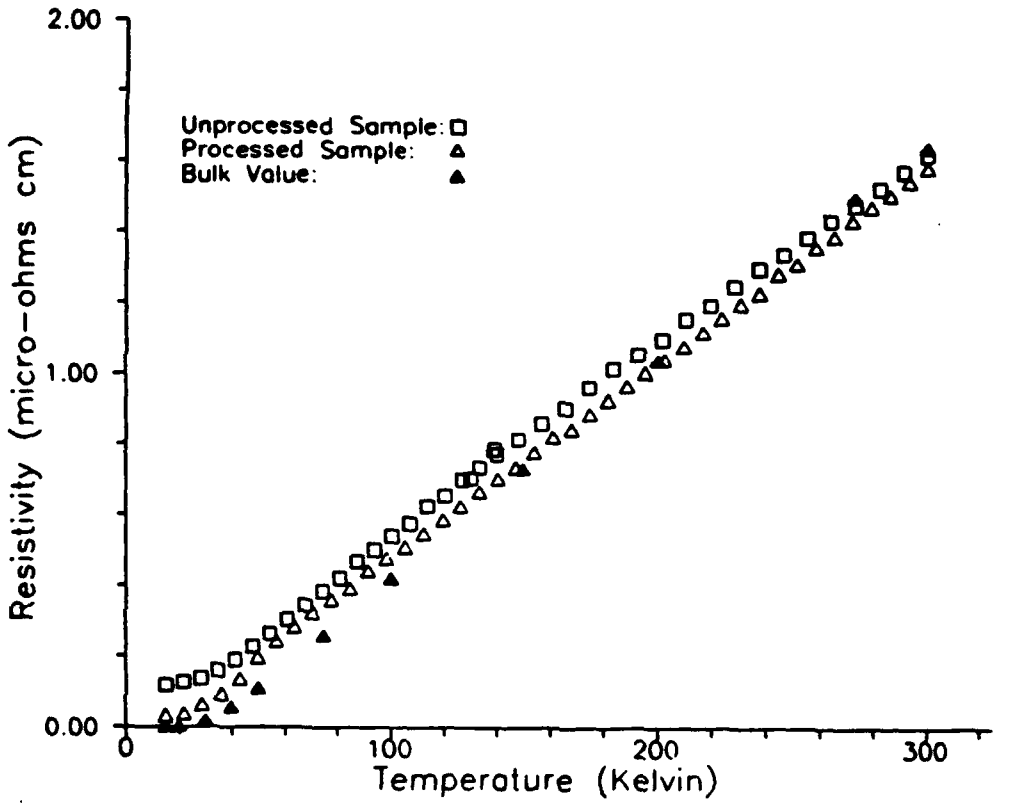

Figure 3.1-5. Temperature dependence of conductivity of electroplated film.

Conclusions and Unresolved Questions

In all three evaluations - conductivity, residual stress, and purity - the silver electroplated with the additive-free $KAg(CN)_2$ solution performed exemplary. First, the conductivity was reproducibly 95% of bulk as plated, and thermal processing under both dry and wet conditions consistently produced conductivities at 100% of bulk. Second, the final residual stress of the electroplated silver was markedly lower than the residual stress magnitudes for gold, aluminum, and copper. Third, the electroplated silver was extremely pure, displaying a linear temperature-conductivity relationship down to as low as 20 K. Furthermore, the electroplated silver was superior in several ways over its sputtered corollary. The as-deposited as well as the processed conductivity of the film was higher in both cases for the electroplated silver, while the residual stress of the electroplated film was but a third of the sputtered film.

Numerous questions remain unanswered. The most important question is the reliability of silver-insulator structures, as used in high performance packaging. This will be investigated in the next 12 months. Experiments have been designed, and facilities are in place.

There are several processing questions which are also under investigation. First, the low temperature purity evaluation for the sputtered silver remains to be accomplished. Second, the exact mechanism by which the conductivity of the films increases during the heat treatment should be discovered. Third, the precise reasons why the electroplated silver has a lower conductivity, both as-deposited and after thermal processing, than the sputtered silver needs to be looked at, as well as the reasons why the sputtered silver reaches the conductivity plateau that it does. Finally, the stark difference between the final stress values of the two silver films, as well as the overall curve shapes, should also be explained.

3.2 Adhesion to Noble Metals

Motivation and Summary:

Group 1B metal films (copper, silver and gold) are attractive for metallizations in MCMs because they have high electrical conductivities. Unfortunately, Group 1B metals require additional bonding layers for adhesion to insulators (i.e. silicon dioxide or polymers). In this study, thin, electrically insulating films of titanium oxide on titanium have been investigated and shown to be an effective adhesion layer between gold and a wide variety of insulators. The adhesion layer does not alter the dielectric properties of the insulator surrounding the metal because it is thin, and is very simple and inexpensive to process.

Method of Analysis:

MCM test structures consisting of gold (or copper) on SiO_2 were fabricated. the adhesion was tested by subjecting the samples to thermal shock (liquid to liquid, 77 K to 373 K), and tape tests. The morphology, composition, and resistivity of the titanium oxide films were studied with angle resolved X-ray Photoelectron Spectroscopy (XPS), Scanning Tunneling Microscopy (STM), and electrical resistance measurements.

Results:

The results show that the sputter-deposited titanium films grow by an island growth (Volmer-Weber) mechanism, as summarized in Fig. 3.2-1. The islands coalesce after 10-20 Å of titanium deposition. Following deposition, the titanium films were oxidized by exposure to air at relatively low temperatures ($T < 100$ °C). Very thin titanium films (3 Å) oxidized completely. When thin titanium films (10-20 Å) were oxidized, a layered film formed with a suboxide (TiO) core and a titanium dioxide surface layer. When thicker films (>20 Å) were oxidized, a layered film was also produced with a titanium core and titanium oxide surface layer.

In this work, angle resolved XPS and STM were used to distinguish between the film growth mechanisms. A layer-by-layer growth model for angle resolved XPS was contrasted to that of an island growth model. The XPS intensity from the gold samples covered with an overlayer material was

measured as a function of photoelectron take-off angle, θ. Fig. 3.2-2 shows the fit of the data to the island and uniform growth models. The STM images confirmed the growth mechanism.

The electrical resistance between two 3.5 cm long electrodes with 40 μm spacing and titanium overcoat thicknesses of 10, 20, and 30 Å were measured after heat treatment in air at 95 °C (45% relative humidity measured at 20 °C) for 0, 5, and 10 minutes. The maximum DC resistance of the meter was 1 Gigaohm. The resistivity of the titanium films was calculated, $R=\rho L/A$, where R is the measured resistance (ohms), ρ is the resistivity (ohm-cm), L is the distance between the anodes (cm), and A is the cross-sectional area (thickness times electrode length) of the film (cm^2). As the film thickness increased from 10 to 30 Å, the resistivity significantly decreased, as shown in Table 3.2-1. Second, the resistivity of each film increased with air exposure time at 95 °C. With a ten minute exposure to air at 95 °C, the resistance of the 10 and 20 Å thick films was greater than 1 Gigaohm, the meter's limit. For the 10 Å film, a 5 minute exposure was sufficient to produce greater than a Gigaohm resistance.

These results show that oxidation of 10 and 20 Å films for 10 minutes was sufficient to convert the titanium conductive path to a non-conductive path (i.e. titanium oxide). If the films were grown with an island growth mechanism, oxidation of the outer shell of the titanium islands would have adequately eliminated any conductive paths, whereas with a layer-by-layer growth mechanism, the bulk of the film would have been oxidized. Thicker films (30 Å) are either not completely oxidized, or the voids between the islands are filled with metal causing an increase in the conductivity.

The adhesion was demonstrated by thermal shock (77 K to 373 K, liquid to liquid, 40 cycles), and tape testing. Titanium thinknesses of 3Å were not adequate for adhesion and delamination of a 5 μm thick film on Au was observed after 10 thermal shock cycles. For thicknesses greater than 6Å, no delamination was observed.

These results show how the adhesion layer functions. The metal core layer bonds to the gold substrate. Even though only thin layers are used, the adhesive layer in the monolayer closest to the gold is adequate for bonding. Because the layers are very thin, the electrical effects of TiO_2 are negligible on the properties of the metals and insulators. Although thin layers of an adhesive material are adequate for adhesion, the ability of titanium to diffuse out of gold and form a potential-sink oxide is essential. In contrast to this behavior, very

thin films of metals and metal-oxides which prefer to reside within the substrate (for example at grain boundaries) would not be expected to serve as long-term adhesion layers. Lastly, the titanium oxide and titanium metal strongly adhere to each other because the titanium oxide is grown at low temperature. Titanium oxide grown at high temperatures is susceptible to cracking, flaking and oxide/metal separation.

Table 3.2-1

Oxidized at 95 °C	Unit	10 Å Ti	20 Å Ti	30 Å Ti
0 minutes	R(Ω)	1.70×10^8	160,000	10
	ρ(Ω-cm)	14,900	28	0.0026
5 minutes	R(Ω)	$>9.99 \times 10^8$	1.30×10^8	51.6
	ρ(Ω-cm)	>87,400	29,600	0.0144
10 minutes	R(Ω)	$>9.99 \times 10^8$	$>9.99 \times 10^8$	100
	ρ(Ω-cm)	>87,400	>175,000	0.0260

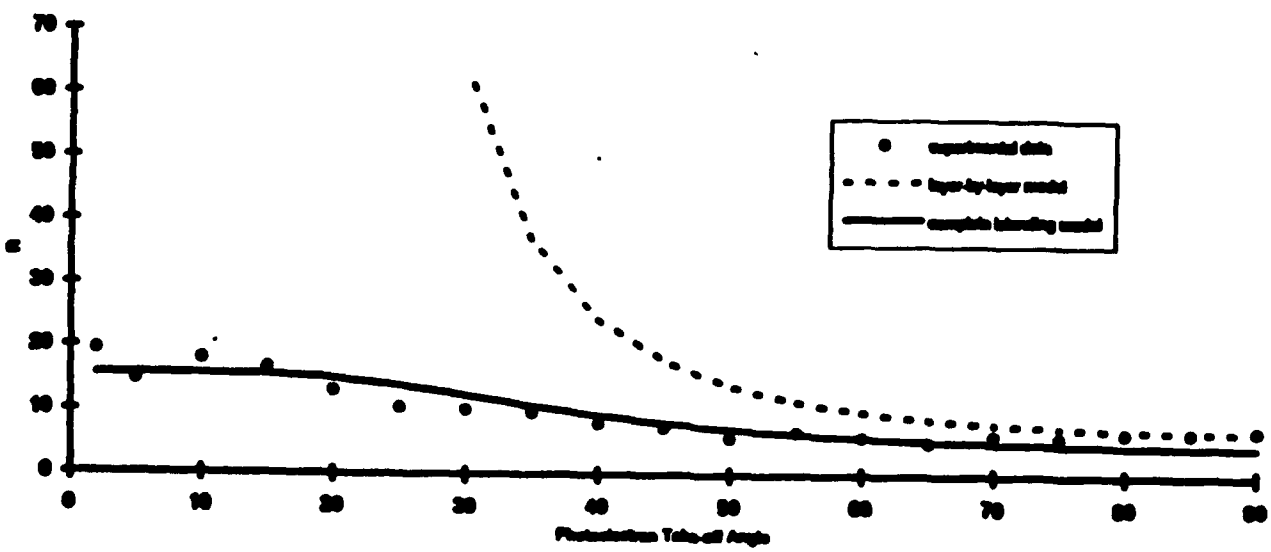

Figure 3.2-2 ARXPS Model Fit for 10 A Ti on a Au-Si Substrate

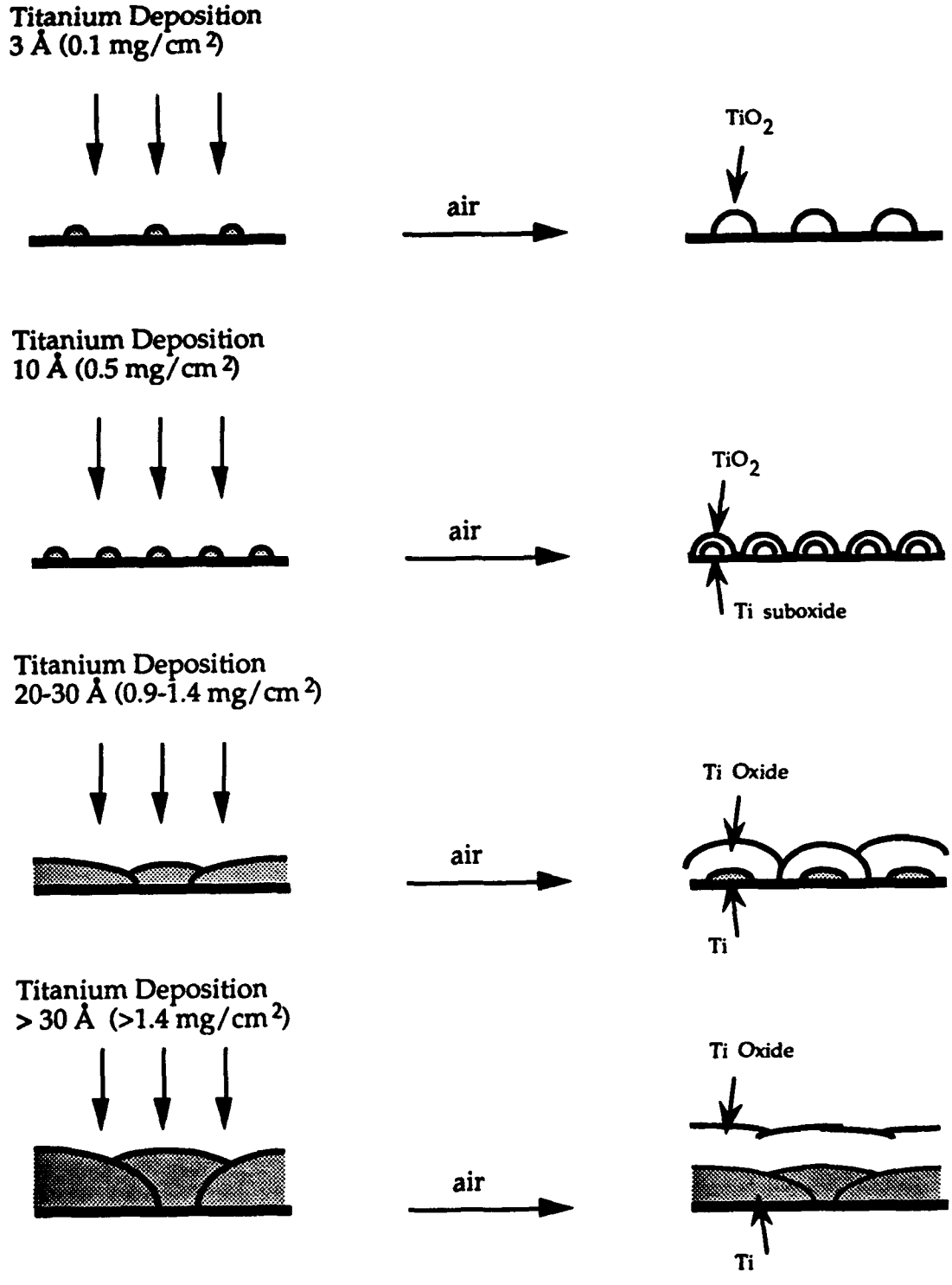

Figure 3.2-1: Composition and morphology summary for the thin titanium adhesion layers.

3.3 Electroless Deposition of Gold

In the production of multichip modules, electroless plating is a common approach to filling level to level via connections. The only electroless baths known to autocatalytically deposit gold operate at pH > 13. Polymers used in processing multichip modules degrade in such basic solutions. This research concentrates on developing electroless baths for the autocatalytic deposition of gold in pH < 10 solutions.

Technical Approach

The goal of this research is to produce and understand electroless gold plating baths which autocatalytically deposit gold at a rate of 0.5 - 10 μm/hr and are compatible with polymer dielectrics, silicon dioxide and photoresist. The electroless plating of gold is a heterogeneous deposition reaction catalyzed by the initial and deposited gold surfaces. The homogeneous production of gold throughout the solution is an undesirable reaction. Other considerations in developing an electroless gold plating bath include the stability of the bath and the deposition rate. This investigation includes understanding the mechanisms involved in the gold deposition, as well as the effect of solution parameters, such as temperature, pH and composition on these mechanisms.

The electroless plating proceeds as two simultaneous reactions on the gold surface: the reduction of the gold complex to gold and the oxidation of a reducing agent.

The oxidation reaction: $R \longrightarrow R^{n} + ne^{-}$

The gold (I) reduction reaction: $AuL_m^{n} + e^{-} \longrightarrow Au + mL^{(n-1)/m}$

R is the reductant, R^{+n} is the oxidized species, AuL_m^{n} is the metal complex with $L^{(n-1)/m}$ being the ligand and n is the number of electrons transferred. The overall deposition reaction can be explained using these partial reactions and the mixed potential theory. The mixed potential theory states that the partial reactions occur simultaneously at a mixed potential, E_m^{0}. The criteria for using the mixed potential theory is that the redox potential of the reductant must be more negative than the reduction

potential of the metal deposition and that the oxidation must proceed catalytically. If the redox potential of the reductant is more positive than the reduction potential of the gold complex, no deposition of gold occurs. If the reducing agent is not catalytically oxidized on the gold, homogeneous reduction of gold occurs throughout the solution The redox potential of the oxidation and reduction reactions are a function of pH, temperature and composition of the bath.

In this project, the use of gold (I) thiosulfate, a stable gold complex, is investigated as a substitute for gold (I) cyanide. The investigation of the reduction mechanism of gold (I) thiosulfate has currently been focused on determining the reduction products using a rotating ring-disk electrode. Electroless baths have been prepared to determine the best reducing agent, gold complex, temperature and pH of the gold solution for depositing adhesive, uniform gold at 0.5-10 μm/hr.

Results

Three possible products of the gold thiosulfate reaction are thiosulfate, sulfite and dithionite. The oxidation of these sulfur species were investigated in order to identify the reduction products. The oxidation of thiosulfate on Pt at pH = 9.2, 25 °C appeared as a kinetically limited reaction dependent upon concentration. At a stationary Pt electrode, thiosulfate oxidized at 0.75 V vs. SCE. At a rotating electrode, the oxidation current was independent of rotation rate. The oxidation of sulfite on Pt at pH = 9.2, 25 °C was diffusion limited and concentration dependent. As the rotation speed of the rotating Pt electrode increased, the oxidation current increased and the oxidation potential became more positive. At 0 RPM and 100 mV/s, sulfite oxidized at 0.7 V vs. SCE. The oxidation of dithionite on Pt at pH = 9.2, 25 °C was diffusion limited and concentration dependent, as well. The oxidation of dithionite is very complicated and involves more than one electron transfer reaction. Dithionite began to oxidize well negative of 0.0 V vs. SCE.

A rotating ring-disk electrode experiment identified thiosulfate as the reduction product of the gold thiosulfate reduction on gold. In the absence of reduction products, the oxidation of gold thiosulfate at the ring electrode was practically identical to the oxidation of thiosulfate on Au, Pt and Hg electrodes. In the presence of the reduction product, thiosulfate,

the oxidation at the ring electrode appeared as the sum of the oxidation of gold thiosulfate and the oxidation of the produced thiosulfate.

On the mercury ring electrode, the oxidation of thiosulfate was quasi-reversible at pH = 9.2 and 25 °C. This one electron transfer reaction was kinetically limited with forward and backward rate constants of 7.37 x 10^{-3} cm/mol s and 1.33 x 10^{-5} cm/mol s, respectively. The oxidation current at 0.05 V vs. SCE was linearly proportional to concentration and to the square root of the sweep rate. The diffusion coefficient of thiosulfate was calculated to be 1.91 x 10^{-5} cm^2/s.

The oxidation of gold thiosulfate at pH = 9.2 and 25 °C on Hg ring electrode was identified as a CE_i mechanism (chemical reaction followed by an irreversible electron transfer reaction) a chemical equilibrium reaction preceding an irreversible electron transfer reaction:

$$Y \underset{k_b}{\overset{k_f}{<==>}} R \qquad K = k_f/k_b$$

$$R \xrightarrow{\quad} R^{+n} + ne^-$$

where R represents thiosulfate. The apparent number of electrons times the transfer coefficient is 0.69. By fitting the data to theory, $K(k_f + k_b)^{1/2}$ equals 5.47 $(cm/mol\ s)^{1/2}$ (where k_f and k_b are the rate constants for the forward and backward reactions).

The reduction of gold thiosulfate on a Au electrode at pH = 9.2, 25 °C was diffusion limited and dependent on concentration and sweep rate. Gold thiosulfate reduced at -0.15 V vs. SCE on a stationary Au electrode at 100 mV/s, 25 °C and pH = 9.2. The reduction of gold thiosulfate on a gold disk electrode was a CE_i mechanism:

$$Au^+ + 2S_2O_3^{-2} \underset{k_b}{\overset{k_f}{<==>}} Au(S_2O_3)_2^{-3}$$

$$Au^+ + e \xrightarrow{\quad} Au$$

where $K = k_f/k_b$ is very large. The apparent number of electrons times the transfer coefficient is 0.222. The calculated value of $K(k_f + k_b)^{1/2}$ is 2.34 $(cm/\ mol\ s)^{1/2}$. The diffusion coefficient for gold thiosulfate is found to be 1.4 x 10^{-5} cm^2/s.

Several electroless baths have been prepared and tested to determine likely reducing agents and preferable pH and temperature conditions of the bath for autocatalytic deposition of gold. The following reducing agents

were tested: ascorbic acid, borohydride, dithionite, hydroxylamine, hydrazine, hypophosphite, and thiourea. Two gold complexes were tested: potassium gold (I) cyanide and sodium gold (I) thiosulfate. None of the above reducing agents reduced gold (I) cyanide to gold at pH = 7.2 - 9.2 and 25 - 65 C. The best reducing agents for gold (I) thiosulfate were ascorbic acid, hydroxylamine and hydrazine. The mixed potential theory predicted deposition rates for these systems at 25 °C. At pH = 7.2, the predicted deposition rates for ascorbic acid, hydroxylamine and hydrazine were 3, 2.4 and 4.5 kA/hr, respectively. The actual deposition rates were 3.3, 1.4 and 1.8 kA/hr, respectively. At pH = 9.2, the predicted deposition rates for ascorbic acid, hydroxylamine and hydrazine were 4.2, 3.6 and 4.8 kA/hr, respectively. The actual deposition rates were 3.7, 2.0 and 2.3 kA/hr, respectively. Application of the mixed potential theory gave more accurate results for the ascorbic acid system than for the hydroxylamine and hydrazine systems. One reason for this discrepancy is that the catalytic properties of the smooth gold electrode surface may be different from the catalytic properties of a deposited gold surface for a particular oxidation reaction. Therefore, the deposition rate on a deposited gold surface would differ from the predicted value and depend upon the kinetic characteristics of the oxidation of the reducing agent.

A comprehensive table of results for the ascorbic acid, hydroxylamine and hydrazine electroless baths at pH = 7.2 - 9.2 and 25 °C - 65 °C is in Table 3.3-1. Ascorbic acid consistently had larger deposition rates and better uniformity than hydroxylamine and hydrazine. The scotch tape test was used to quantify the adhesive quality of the deposited gold. The percentage of the tested area removed by the tape is recorded in Table 3.3-1. All of the systems listed in this table had very adhesive gold deposited.

The effects of temperature and pH on the ascorbic acid / gold thiosulfate electroless bath were investigated. The deposition rates, adhesion performance and comments on the stability of the bath consisting of .01 M ascorbic acid and .01 M gold thiosulfate are in Table 3.3-2. The deposition rates were highest for pH = 7.2 and increased with temperature. However, the reduction of gold became more homogeneous as the pH and temperature increased. Reduced factorial experiments are presently being performed to determine which variables have the greatest effect on the

deposition rate and bath stability. Results from these tests will aid in designing an optimum ascorbic acid / gold thiosulfate electroless bath.

Conclusion

The investigation of the gold thiosulfate reduction reaction is ongoing. Characteristic curves of the oxidation of gold thiosulfate, thiosulfate, sulfite, dithionite and the reduction of gold thiosulfate have been obtained. Thiosulfate has been identified as the product of the gold thiosulfate reduction reaction. In electroless baths, gold thiosulfate is autocatalytically reduced on a gold surface by the following reducing agents: ascorbic acid, hydrazine and hydroxylamine. These reducing agents, as well as borohydride, dithionite, hypophosphite and thiourea, failed to autocatalytically deposit gold in electroless baths containing gold cyanide. The electroless bath consisting of ascorbic acid and gold thiosulfate is being further investigated.

Table 3.3-1
Effect of Reducing Agent, T and pH on Electroless Bath Behavior

Reducing Agent	T	pH	Dep. Rate	Adhesion	Comments
	°C		kA/hr	% Removed	
Ascorbic Acid	25	7.2	3.32	0	Good Uniformity
Ascorbic Acid	35	7.2	13.37	0	Fair Uniformity
Ascorbic Acid	25	9.2	3.70	0	Good Uniformity
Ascorbic Acid	35	9.2	4.50	0	Good Uniformity
Hydroxylamine	25	7.2	1.42	0	Bad Uniformity
Hydroxylamine	35	7.2	6.83	0	Fair Uniformity
Hydroxylamine	25	9.2	2.00	0	Good Uniformity
Hydroxylamine	35	9.2	3.60	0	Good Uniformity
Hydrazine	25	7.2	4.50	0	Good Uniformity
Hydrazine	35	7.2	3.12	0	Fair Uniformity
Hydrazine	25	9.2	2.29	0	Good Uniformity
Hydrazine	35	9.2	2.44	0	Good Uniformity

Table 3.3-2
Effect of T and pH on Electroless Bath Behavior
.01 M Ascorbic Acid + .01 M Gold Thiosulfate

pH	T	Dep. Rate	Adhesion	Comments
	°C	kA/hr	% Removed	
6.4	25	5.95	0	heterogeneous reduction of gold
6.4	45	9.51	0	slight homogeneous reduction of gold
7.2	25	2.77	0	heterogeneous reduction of gold
7.2	35	12.10	0	slight homogeneous reduction of gold
7.2	45	14.12	0	homogeneous reduction of gold
9.2	25	3.87	0	slight homogeneous reduction of gold
9.2	35	3.90	0	homogeneous reduction of gold
9.2	45	4.67	0	homogeneous reduction of gold

3.4 Electromigration Studies

Polyimide has excellent chemical and electrical properties; however, polyimide has the tendency to absorb moisture. The possible degradation of the electrical properties of polyimide due to moisture absorption causes concern for long-term reliability in integrated circuits. It is therefore in our intention to determine if polyimide can retain its insulating properties under high humidity conditions to prevent electromigration on silver lines.

Electromigration studies will be performed on silver lines insulated with polyimide. Since device lifetime is dependent on geometry and line environment, non-insulated aluminum lines will be studied also, to determine device lifetime of exposed silver lines.

Device lifetime for electromigration is a function of stressing conditions given by the Black equation [3.1-1]:

$$1/MTF = A\, j^n \exp(Ea/RT) \qquad (1)$$

where MTF is mean time to failure, j is current density, n is the exponent which shows failure dependence on current density, Ea is activation energy of diffusion that brings the conductor to failure, and A is the pre-exponential factor dependent on conductor width and film thickness. Once these parameters are found for the silver lines, the data will be extrapolated to find device lifetime under normal operation. In addition to the conventional electromigration, "ionic migration" or dentrilic growth between conductors is being investigated.

Electromigration studies of gold lines are currently in progress. The line width ranges from 12-50 microns, and the average line length is 1 cm. A potential of 10 V is applied across the lines, and a 1000 ohm resistor is connected in parallel. In order to control the device environment, the devices are exposed in a Blue M Humidity Chamber to 85°C and 85% relative humidity. Weight changes due to moisture absorption are measured using a Cahn Microbalance. Although we expect to observe no electromigration on the gold lines, this preliminary study will aid us in determining how applicable the current experimental setup is to the study for the silver lines.

4. Low Dielectric Constant Polymers

4.1 Polyimides and Bis-Benzocyclobutene

The goal of this portion of the program is to determine the polymeric insulating material with the best trade-off between low dielectric constant, low moisture absorption, low residual stress, and thermal expansion matched to the underlying substrate material for use as an interlevel dielectric in high frequency MCMs. For this purpose, a list of ten commercially available polymeric materials were selected for testing (see Table 4.1-1). An ideal material would have a dielectric constant less than 3.0 from 1 kHz to 10 GHz, have no residual stress, have no orientation variation (as indicated by the birefringence), no moisture absorption, excellent adhesion and no interaction with all other materials in the MCM structure, and be inexpensive. No existing material fulfills all of these criteria, so a trade-off between these desired properties must be made. For this reason a number of different polymer chemistries need to be examined before an informed decision can be made.

This work constitutes the core of the program and is still in progress. However, significant work has been completed. Values for low frequency (1-100 kHz) dielectric constant, room temperature residual stress, refractive index and birefringence have been measured and are shown in Table 4.1-1. An example of how the trade-off between properties is important is illustrated by PI-2611. This polyimide material has a very low residual stress and a very low in-plane coefficient of thermal expansion (CTE); however, the birefringence of this material is very high. The high birefringence indicates that the polymer chains are oriented in the plane of the film and that the polymer will have significant differences in electrical and mechanical properties between the in-plane and through-plane directions. One study on a similar polyimide indicates that while the through-plane dielectric constant is about 3.0, the in-plane dielectric constant may be as high as 3.5 [4.1-1]. Thus a material with excellent properties in some respects, may not be the best overall choice. Measurements of the mechanical, thermal and electrical properties in the in-plane and through-plane directions will be performed as part of this program in the near future. Also, moisture uptake experiments remain to be performed.

Interactions of the polymer insulator with the metal conducting lines is a significant factor in the reliability and performance of MCMs. Adhesion between

the two materials must be high to prevent failure due to thermal expansion mismatch. Two materials, DuPont PI-2611 and Dow BCB, were spin coated on silver and gold sputtered silicon wafers. A 20 Å titanium adhesion layer was applied to the metal surface prior to polymer coating. All of these material combinations withstood 50 cycles from boiling water to liquid nitrogen and back to boiling water without delamination occuring between the polymer and the metal surface. This result is vitally important to the success of production of noble metal MCMs using polymeric insulators.

4.2 Polyquinoline

Polyquinoline was initially of interest for use in GHz multi-chip modules because of its low dielectric constant (~2.7 - 2.9) and because of its reported low residual stress. Stress measurement performed in our laboratory indicated that the residual stress was ~40 MPa, in the same range of that for many polyimides. The lower curing temperatures required for polyquinoline can be a potential asset in certain applications.

The dielectric properties of polyquinoline films cured at different temperatures were examined. Since the recommended cure temperature for this polymer was 350°C for 1 hour in nitrogen, the effects of overcuring and undercuring were of interest. A value of approximately 2.9 at 100 kHz for the permittivity was obtained with films cured at 250°C, 350°C, and 400°C. According to the manufacturer, only slight crosslinking occurs during the baking step. Since no major chemical changes occur through hardbaking, similar dielectric properties were obtained for the overbaked and the underbaked polymer films.

The effect of cure temperature on the residual stress in the polymer was also explored. The results are summarized in Table 4.2-1. The wafer processed at 200°C had a stress value around 30 MPa (at 25°C). The films cured at 250°C, 350°C, and 400°C show stress values that are similar to each other, approximately 40 MPa. It is possible that the light crosslinking which occurs at the high temperatures is responsible for changing the mechanical properties of the films. As the polymer chains crosslink, their mobility becomes restricted, leading to the increase in residual stress. There is no crosslinking in the film processed at 200°C, hence the lower stress. The increased freedom for the chain segment mobility allows for the relief of the stress.

These results indicate that polyquinoline films may be processed at lower temperatures, in order to lower the stress in the wafer, without substantial effect on the permittivity. However, solvent resistance may be reduced in the films cured at lower temperature because there was no crosslinking of the polymer chains. This may be an important factor if further processing steps are required. Photoresists, developing solutions, or wet etching solutions may dissolve or deform the polymer film with which they come in contact.

Work is in progress to measure the CTE, and the dielectric properties as well as the solvent resistance in order to fully characterize this polymer. So far, BCB seems to exhibit similar, if not better, characteristics, both mechanical and electrical.

Table 4.2-1: Summary of the Effect of Cure Temperature on Moisture and Stress for Maxdem Polyquinoline

Final Cure Temperature (°C)	Permittivity	Stress (MPa)
200	2.8	29.1
250	2.9	39.8
350	3.0	38.7
400	2.9	39.6

Table 4.1-1 Polymers under test and results to date.

Polymer	Manufacturer	Special Properties	Dielectric Constant	Residual Stress (MPa)	Refractive Index	Birefringence	Cure Temp. (°C)
PI-2545	DuPont	Low cost, common material	3.3-3.5	25	1.726	0.093	350
PI-2555	DuPont	Low cost	3.1-3.3	35	1.686	0.017	350
PI-2566	DuPont	Fluorinated	2.95-3.05	38	1.591	0.010	350
PI-2611	DuPont	Rigid Rod	2.9-3.1	5	1.845	0.230	350
PIQ-L100	Hitachi	Rigid Rod	3.0-3.1	1.5	1.840	0.216	350
EL-5010	Nat'l Starch	Thermoset Polyimide	3.3-3.5	35	1.686	0.007	400
EL-5512	Nat'l Starch	Fluorinated Thermoset Polyimide	2.9-3.0	42	1.616	0.005	400
PB 293	OCG	Preimidized	3.1-3.2	35	1.635	0.023	250
U-4208	Amoco		2.95-3.05	32	1.614	0.012	350
Benzocyclobutene (BCB)	Dow	Nonpolyimide No moisture produced	2.6-2.9	30	1.551	0.002	250

4.3 Rapid Processing of Polymer Dielectrics

Polymer dielectric films currently are cured in inert gas purged furnaces requiring long heating and cooling times to reach the polymer cure temperature. Logistics problems are created because the long cure time requires that the wafers be batched, increasing the work-in-progress and intermixing continuous (i.e., single wafer) and batch processes. In order to provide adequate throughput, a large capital expenditure for multiple furnaces must be made. Also, the cost of operating a large number of furnaces must include the increased load on the clean room air handling system.

In this work, an alternative polymer cure schedule is proposed using automated microelectronic fabrication equipment with the goal of reducing the curing time to that compatible with continuous, photoresist processing. Photoresist can be more rapidly baked using hot plate heating than by convection/radiation heating. [4.3-1] A similar, rapid process sequence was investigated for processing interlevel dielectric polymers using photoresist spin-coating and hot plate baking Flexifab modules, manufactured by Machine Technology, Inc. (MTI, Parsipanny, NJ), modified to provide a nitrogen atmosphere during curing. The potential actions involved in polymer curing are solvent evolution, similar to photoresist baking; ring closing reactions, e.g., polyimides; and, chain cross linking. Hot plate curing should provide good solvent removal since the heat is applied from the bottom (wafer) side of the film.

This work examined representative materials from three different classes of commercially available polymer systems for their compatibility with rapid cure processing: condensation polyimides (polyamic acid-based materials), preimidized polyimides, and benzocyclobutene. The rapid cure film properties were compared with the properties of films cured by traditional, batch furnace cure cycles.

The criteria for quality of the polymer films was quantified by measuring the permittivity, loss factor, residual stress, birefringence, and solvent resistance. These properties are all affected by the polymer chemistry, the extent of curing and the presence of residual solvent in the film. All measurements were made in-situ on polymer films spin-coated on silicon substrates. Permittivity and loss measurements were performed at 10 kHz on parallel plate capacitors using a Hewlett-Packard 4263A LCR meter and a probe station. Residual stress was determined using a Flexus F2320 Stress Analysis system (Tencor Instruments Co., Sunnyvale, CA). [4.3-2] and the birefringence was determined using a Metricon

2010 Prism Coupler system (Metricon Corp., Pennington, NJ). [4.3-3] A Nicolet 520 FT-IR spectrometer was used for comparison of the chemical structure of the furnace cured and rapidly cured films.

DuPont PI-2545 (pyromellitic dianhydride-oxydianiline or PMDA-ODA) is a polyamic acid-based polyimide that undergoes a ring closure imidization reaction during cure which produces water as a by-product. The polymer is supplied as a B-staged polyamic acid solution in N-methyl pyrrolidone (NMP) solvent. Since water is produced during reaction, it is possible to entrap polar water molecules in the fully cured film which would seriously degrade the dielectric properties of the polymer. Also during cure, polyimide chains tend to rearrange with their long axis in the plane of the film to achieve a lower stress film. [4.3-4] Sufficient cure time must be allowed for the generated water to diffuse out of the film and for the chain segments to reorient to a lower stress conformation. In addition, the extent of reaction and reaction time are critical to the performance properties of PMDA-ODA. The FT-IR spectra of the rapidly cured films and the furnace cured film contain all of the peaks typical of cured PMDA-ODA, indicating that the rapidly cured films did imidize and that negligible amounts of water and residual solvent were present. [4.3-5] The refractive indices, birefringence, residual stress, permittivity and loss factor at 25°C of PMDA-ODA films cured at 350°C for 30 seconds, 2 minutes and by a 350°C furnace cure cycle are shown in Table 4.3-1. The properties of the rapidly cured films are significantly different from those of the furnace cured sample, indicating a less oriented polymer film. This result is consistent with work performed by Pottinger and Coburn for the rapid heating of polyamic acid. [4.3-6]

OCG Probimide 293 (Pyromellitic dianhydride - oxydianiline - 5(6)-amino-1-(4-aminophenyl)-1,3,3-trimethylindane or PMDA-ODA-DAPI) is representative of preimidized polyimides. The polymer is provided as a soluble, fully imidized polyimide suspended in NMP. Since imidization has already been completed, the heating of this material consists only of the simple release of solvent. Previous work with Probimide 293 has shown a crosslinking reaction at elevated temperatures (above 300°C), improving the film solvent resistance. [4] Samples cured over a range of temperatures from 200°C to 350°C were tested for resistance to γ-BL and to NMP with results shown in Table 4.3-2. Resistance to γ-BL is poor for all samples cured at 300°C and below, failing in one minute or less because the crosslinking reaction has not began. NMP resistance is generally good for all

the samples, with the rapidly cured films showing superior resistance over the furnace cured specimens. These solvent resistance tests indicate that the rapidly cured films have better resistance to solvents, especially when cured at 350°C. The improved solvent resistance at 350°C is desirable in the formation of multilayer structures since the polymer film should be impervious to solvents in subsequent polymer and photoresist depositions.

Birefringence, residual stress and dielectric measurements were performed to compare films produced by rapid curing and furnace curing at 350°C, as shown in Table 4.3-3. All four properties are essentially the same, within experimental error, indicating that the preimidized polyimide can be rapidly cured.

Cyclotene 3022 (Bisdivinylsiloxane benzocyclobutene, BCB, manufactured by Dow Chemical,Co.) is a thermosetting non-polyimide. The benzocyclobutene reaction does not involve diffusion and no volatiles are produced during cure. [4.3-7] As with the polyimide systems, solvent removal from the benzocyclobutene film will be critical to the resulting film quality. A reaction rate versus temperature curve for BCB at various extents of cure has been produced by Heistand et al. [4.3-8] They have shown that the cure time can be reduced by increasing the temperature. BCB films were cured over a range of times and temperatures ranging from six seconds at 305°C to fifteen seconds at 275°C. The extent of cure for each of these samples was determined by FT-IR and is listed in Table 4.3-4. The percent cure matched very closely with the conversion predicted by Heistand et al under the same conditions. [4.3-8] These results confirm that the extent of cure may be controlled by varying either the cure temperature or the cure time. The extent of reaction is particularly sensitive to temperature in the short cure time, high temperature regime. Over a range of 10°C (from 275°C to 285°C), the extent of cure rose almost 18% (from 62.8% at 275°C to 81% at 285°C). This result indicates that very good temperature control is necessary to obtain consistent film curing between wafers. In addition, the FT-IR results show that the rapidly cured films have the same chemical composition as the furnace cured samples and are unoxidized.

The birefringence, residual stress, and dielectric properties are listed in Table 4.3-4. The rapidly cured samples exhibit a small, but essentially insignificant, increase in birefringence. The measured stresses agree with observations made by Heistand et al on stress as a function of extent of cure for BCB. [4.3-8] The dielectric properties are all within experimental error, yielding a

permittivity of about 2.8 and a loss factor of 0.007. The stable dielectric properties combined with the similar film stresses for the rapidly cured and furnace cured samples indicate that the BCB films have properties consistent with the extent of conversion, regardless of the cure method used.

Rapid processing of polymer dielectrics has been shown to be a viable process using existing fabrication equipment. Fast, hot plate curing was demonstrated to yield polymer films which were equivalent to those produced by standard, furnace curing processes for benzocyclobutene and preimidized polyimide. Polyamic acid-based polyimides were shown to be incompatible with rapid, hot plate curing techniques due to the inferior properties of the resulting films compared to furnace cured material.

Results of this work have been submitted for publication in the *International Journal of Microcircuits and Packaging Technology*.

Table 4.3-1. Comparison of PMDA-ODA Cure Conditions

Cure Condition	In-Plane Refractive Index	Through-Plane Refractive Index	Birefringence	Residual Stress (MPa)	Permittivity	Loss Factor
30 sec@350°C	1.712	1.675	0.0347	53.1	3.41	0.004
2 min@350°C	1.712	1.676	0.0358	51.6	3.41	0.004
350°C Furnace Cure	1.728	1.637	0.0958	22.9	3.25	0.003

Table 4.3-2. Solvent resistance of Preimidized Polyimide.

	Solvent	Resistance
Cure Conditions	**-Butyrolactone**	**N-Methyl Pyrrolidone**
5 sec @ 200°C	1 min	10 sec
2 min @ 200°C	1 min	5 min
2 min @ 250°C	1 min	5+ min
2 min @ 300°C	1 min	4+ min
30 sec @ 300°C	1 min	3.5+ min
30 sec @ 350°C	5+ min	5+ min
250°C Furnace Cure	1 min	2 min
350°C Furnace Cure	2 min	5 min

Table 4.3-3. Comparison of Fast Cure and Furnace Cure Preimidized Polyimide

Cure Condition	Birefringence	Residual Stress (MPa)	Permittivity	Loss Factor
30 sec @ 350°C	0.0098	40.3	3.30	0.0041
350°C Furnace Cure	0.0099	41.6	3.31	0.0047

Table 4.3-4. Results of BCB Testing

Cure Conditions	Extent of Cure (%)	Birefringence	Residual Stress (MPa)	Permittivity	Loss Factor
15 sec @ 275°C	62.8	- - -	26.7	- - -	- - -
15 sec @ 280°C	77.0	0.0038	31.0	2.81	0.006
15 sec @ 285°C	81.0	0.0043	32.5	2.79	0.007
13 sec @290°C	84.5	0.0043	34.8	2.80	0.007
6 sec @ 305°C	87.9	0.0045	37.5	2.89	0.008
275°C Furnace Cure	92.3	0.0021	32.5	2.78	0.006

Another problem with the use of benzocyclobutene films is their etching characteristics. The commercially available BCB material is a silicon containing hydrocarbon. BCB will not etch in either a fluorine plasma(as would silicon or silicon dioxide) or in an oxygen plasmas(as would a normal polymer). However, with careful blending of these two gas plasmas we have been able to successfully etch fine via patterns in the BCB dielectric.

Our process utilizes a trilevel structure consisting of a photoresist patterning layer(3 microns thick) and a thin SiO_2 transfer layer (100-2000A thick) over the 4-7 micron thick BCB dielectric. The photoresist is patterned using standard UV lithography techniques. The exposed SiO_2 is then etched in a Fluorine plasma to form the via patterns. The BCB is then etched in a 50:2 O_2CFH_3 plasma. This plasma etches the photoresist off of the SiO_2 layer and also attacks the SiO_2 to a small extent. Following BCB etching the remaining SiO_2 is removed in a fluorine plasma.

The use of this tri-level patterning technique allows the fabrication of interconnection through the BCB which is critical in MCM designs. Results of this work were presented at the VLSI Packaging Workshop in Kyoto, Japan. [4.3-9]

4.4 Moisture Measurements

The presence of moisture in polyimide thin films can affect insulator dielectric properties. We are therefore interested in developing a correlation between moisture uptake and changes in capacitance and dielectric permittivity.

Moisture uptake by polyimide films will be measured using capacitors exposed to various humidity conditions. We expect capacitance to increase appreciably with increased moisture absorption, as well as weight changes to increase significantly at higher humidities.

Comb electrodes of width 12-50 microns insulated with polyimide will be used to determine capacitance changes due to moisture absorption. These electrodes will be exposed in a Blue M Humidity Chamber at 25°C and 20-100% relative humidity. The audio frequency capacitance will be measured at 5% relative humidity intervals. Since the devices are small, we assume that they come to equilibrium with the environment quickly, and that capacitance measurements are made at each percent relative humidity after the polyimide

has reached equilibrium. A Cahn Microbalance supported above the chamber will be used to allow for suspension of the device into the humidity chamber and for continuous weight measurements. A data acquisition system will record weight changes as a function of change in percent relative humidity, and allow for calculation of changes in dielectric permittivity as a function of relative humidity once the capactitance change is known.

The experimental setup is nearly complete, all apparati for the study are readily available. The Cahn Microbalance is in the process of being mounted on a vibration-free shelf above the humidity chamber, and once that is completed, moisture measurements will begin.

4.5 Photosensitive Polyimides

Purpose:

Polyimides are being considered for a variety of MCM and IC applications and a range of photodefinable or photosensitive polyimide formulations have been developed. Photodefinable polyimides can be classified into two major groups: those that require a high temperature cure to convert the photocrosslinked intermediate to the fully imidized final product, and those that are preimidized as well as photosensitive and do not require a high temperature cure. Four commercially available products were evaluated for superior processing, mechanical, and electrical characteristics, Amoco Ultradel 7501, Ciba-Geigy Probimide 349 and 412, and DuPont 2732.

Approach:

The evaluation of each of the three commercial products was organized under three main criteria: processing performance, mechanical performance, and electrical performance. In terms of processing performance, the figures of merit included shelf-life, cost, physical ease and reproducibility of processing, percent shrinkage upon final cure, and via hole wall profiles. In terms of mechanical performance, the figures of merit included the residual stress upon cure, adhesion to gold metalization, degree of planarization, and the percent moisture uptake. And in terms of electrical performance, the figure of merit was mainly the dielectric constant of the material. In every single criteria listed above, the cure cycle played a dominant role in the resulting film properties.

Data and Results

The preliminary results obtained indicate that very little, if any, sacrifices in material performance are endured in return for the convenience of photodefinability.

Ciba-Geigy Probimide 349

In terms of processing performance, the Ciba-Geigy Probimide 349 ranked as the least desirable product. Soft bake times were on the order of two hours, and the soft baked film was very susceptible to damage during the soft contact on the mask aligner. In addition, the wall profiles displayed heavily rounded corners and edges, and wall slopes of better than 60^{o} could not be obtained due to the 55% shrinkage that occurred during the cure. But perhaps the product's worst attribute was its complete opaqueness upon final cure. Even curing the film in a nitrogen atmosphere could not prevent the film from turning such a dark color as to preclude this product from any applications where pattern alignments are required. For this reason, the evaluation of the mechanical and electrical performance of this material was not pursued.

Amoco Ultradel 7501

In terms of overall material performance, the Amoco Ultradel 7501 delivered all the advantages of photodefinability in conjunction with superb processing, mechanical, and electrical characteristics. The spin coatings were effortless and produced very uniform and reproducible films. The shelf-life of this material is indefinitely at 4 ^{o}C, and six months at room temperature. The soft bake times were under twenty minutes, the material displayed excellent adhesion to the gold metalization, and the wall profiles and slopes were sharp and nearly vertical. The sharp, vertical wall profiles were possible due to the less than 10% shrinkage the film experienced during the cure. Above approximately 200 ^{o}C, the percent shrinkage and wall profiles became independent of the final cure temperature. The residual stress proved to be a function of the final cure temperature, with the fully cured, transparent film displaying a residual stress of 42.0 MPa. In addition, upon subsequent reheating cycles the film displayed complete elasticity as long as the highest temperature the film was previously processed at was not exceeded. The dielectric constant of the material also

proved to be a function of the final cure temperature with the fully cured, transparent film displaying a dielectric constant of 3.15.

Ciba-Geigy Probimide 412

In terms of overall material performance, the Ciba-Geigy Probimide 412 also delivered all the advantages of photodefineability in conjunction with superb processing, mechanical, and electrical characteristics. In addition, the preimidized attribute of the product resulted in some very advantageous low temperature processing capabilities. The spin coatings were also effortless and produced uniform and reproducible films. Since the product is preimidized, the shelf-life of this material is indefinitely at room temperature. The soft bake times were also under twenty minutes, the material displayed excellent adhesion to the gold metalization, and the wall profiles and slopes were also sharp and nearly vertical. The sharp, vertical wall profiles were possible due to the less than 10% shrinkage the film experienced in the cure. Above approximately 200 ^{o}C, the percent shrinkage and wall profiles become independent of the final cure temperature. Unlike the Amoco product, the residual stress proved to be nearly independent of the final cure temperature and was measured to be 35.0 MPa. In addition, upon subsequent reheating cycles the film displayed complete elasticity as long as the highest temperature the film was previously processed at was not exceeded. The dielectric constant of the material also proved to be nearly independent of the final cure temperature, and was measured to be 3.15. The fact that the material's residual stress and dielectric constant were nearly independent of the final cure temperature introduces the possibility of low temperature processing with this material that is simply not an option with the non-preimidized materials.

DuPont 2732: the data has not been completed.

Conclusions and Unresolved Questions

The Ciba-Geigy Probimide 349 is not a suitable material for multi-chip modules due to its opaqueness upon final cure. The manufacturer stated that curing in a good vacuum might alleviate this problem, but even if a transparent film could be obtained the poor wall profiles and slopes, as well as the tempermental processing characteristics, preclude its recommendation. The

Amoco Ultradel 7501 and the Ciba-Geigy Probimide 412 both represent all the advantages of a photodefineable product and can match nearly any non-photosensitive product in their processing, mechanical, and electrical properties. However, the preimidized Ciba-Geigy Probimide 412 holds the added dimension of possible low temperature processing, and thus it receives the highest recommendation of the four.

A few questions remain unresolved. First of all, the degree of planarization and percent moisture uptake have yet to be investigated. The percent moisture uptake will be investigated using the films already prepared for the residual stress measurements, and the very low percent shrinkage of the two recommended products almost assures a degree of planarization of nearly 100%. Secondly, residual stress curves for all the materials need to be investigated at low temperatures (around 77K) for applications in high-temperature superconducting devices. Thirdly, complete multi-chip module test structures should be fabricated to explore the electrical properties of the materials in more detail, including the dielectric constant of the materials as a function of water uptake and device temperature. And lastly, the possible problems associated with a multi-layered device using the Ciba-Geigy Probimide 412 needs to be investigated. Since no chemical reaction is taking place during the cure for this preimidized product, subsequent coatings could partially dissolve the bottom layers at the layer interface.

5. Inorganic Insulators

5.1 Silicon Dioxide

Thin silicon dioxide films are commonly used as insulating layers in metal-insulator devices such as integrated circuits and multi-chip modules. These films are either thermally grown through the oxidation of silicon or deposited by thermally or plasma-enhanced CVD. The advantage of PECVD is that lower deposition temperatures can be used avoiding defect formation, diffusion, and degradation of the metal layer, particularly when low melting point substrates or films are present.

PECVD silicon dioxide films contain more silanol (SiOH) and water and are less dense than films deposited or grown at high temperatures. The residual

silanol and water concentrations are therefore the quantities of primary importance when evaluating the film composition. The primary goal of this study was to determine the effect of the silanol concentration on the film properties, including the permittivity, loss, refractive index, wet etch rate, and residual stress. Second, the effects of the deposition parameters including substrate temperature, RF power, pressure, and reactant gas (silane and nitrous oxide) flow rates on the film composition were determined. Thus, the low temperature PECVD conditions that produce silicon dioxide with the film composition and properties most suited for use in metal-insulator structures were determined.

The post-deposition treatment of PECVD silicon dioxide films has also been studied. Plasma-deposited oxides have been treated with nitrous oxide and nitrogen plasmas, with hydrazine in a hot walled CVD reactor, and with low temperature baking. These treatments will to some extent convert the silanol species to oxygen or nitrogen. This should cause a decrease in the silanol concentration of the material. These studies are nearing completion and the presentation of the data will be shortly forthcoming.

The use of spun-on-glass films as interlevel dielectrics has been investigated. Spun-on-glass layers are deposited in the same manner as polymer films, by spin coating and curing. Evaluation of an Allied-Signal developmental polysilsesquioxane was limited because of film cracking. Despite variations in the cure temperature and time, a crack-free spun-on-glass film of sufficient thickness could not be obtained.

Thus, the bulk of the experimental work has involved the investigation of PECVD silicon dioxide. The deposition parameters were varied in an orthogonal array (as shown in Table 5.1-1) to evaluate the effects of the deposition parameters on the film composition and properties.

The effects of the deposition parameters on the silanol and water concentration are shown in Figure 5.1-1. The substrate temperature has the largest effect on the silanol and water impurity concentrations. A thermally activated surface phenomenon inhibits the formation and promotes the removal of impurities causing more complete silicon dioxide bonding (5.1-1). Increasing the RF power increases the level of ion bombardment which increases the rate of surface reactions, increases the mobility of the species on the surface, and enhances the desorption of by-products causing more complete silicon dioxide bonding and lower impurity concentrations (5.1-2). An increase in the reactor

pressure causes an increase in the residence time at a fixed pumping speed. The concentration of oxygen radicals produced in the plasma increases with residence time leading to more complete silicon dioxide bonding and a lower silanol concentration (5.1-3). Changing the reactant gas flow rates changes the relative amounts of the reactants at the surface. Increasing the nitrous oxide to silane ratio causes less complete silicon dioxide bonding and a larger impurity concentration because silane is the limiting reagent (5.1-4).

The silanol concentration is an important factor in determining the film properties. First, the hydroxyl group of the silanol and water are more polar than silicon dioxide. Therefore, an increase in the silanol and water concentration causes an increase the permittivity and loss (Figure 5.1-2 and 5.1-3). Second, the oxide becomes less dense with the inclusion of impurities into the silicon dioxide lattice. Thus, the refractive index decreases as the silanol concentration increases (Figure 5.1-4). Similarly, as the extent of silicon dioxide bonding decreases, the number of bonds that must be broken to etch the film decreases. Thus, the wet etch rate increases as the silanol concentration increases (Figure 5.1-5).

The residual stress of the films at room temperature appears to be independent of the film composition. Increasing the substrate temperature or the RF power increase the residual stress of the film. The pressure and reactant gas flow rates exhibit comparatively small effects on the residual stress.

Thus, the relationships between the film composition, film properties, and deposition parameters have been examined. Although the substrate temperature has the largest effect on the film composition, using a large RF power, high pressure, and low nitrous oxide to silane ratio will minimize the silanol concentration at a given temperature. This, in turn, will minimize the dielectric constant of the oxide produced.

Table 5.1-1. Deposition Parameters

Substrate Temperature	200 - 400 °C
Pressure	0.25 - 1.80 Torr
RF Power	20 - 150 W
2% Silane in Nitrogen Flow Rate	200 - 400 sccm
Nitrous Oxide Flow Rate	400 - 900 sccm

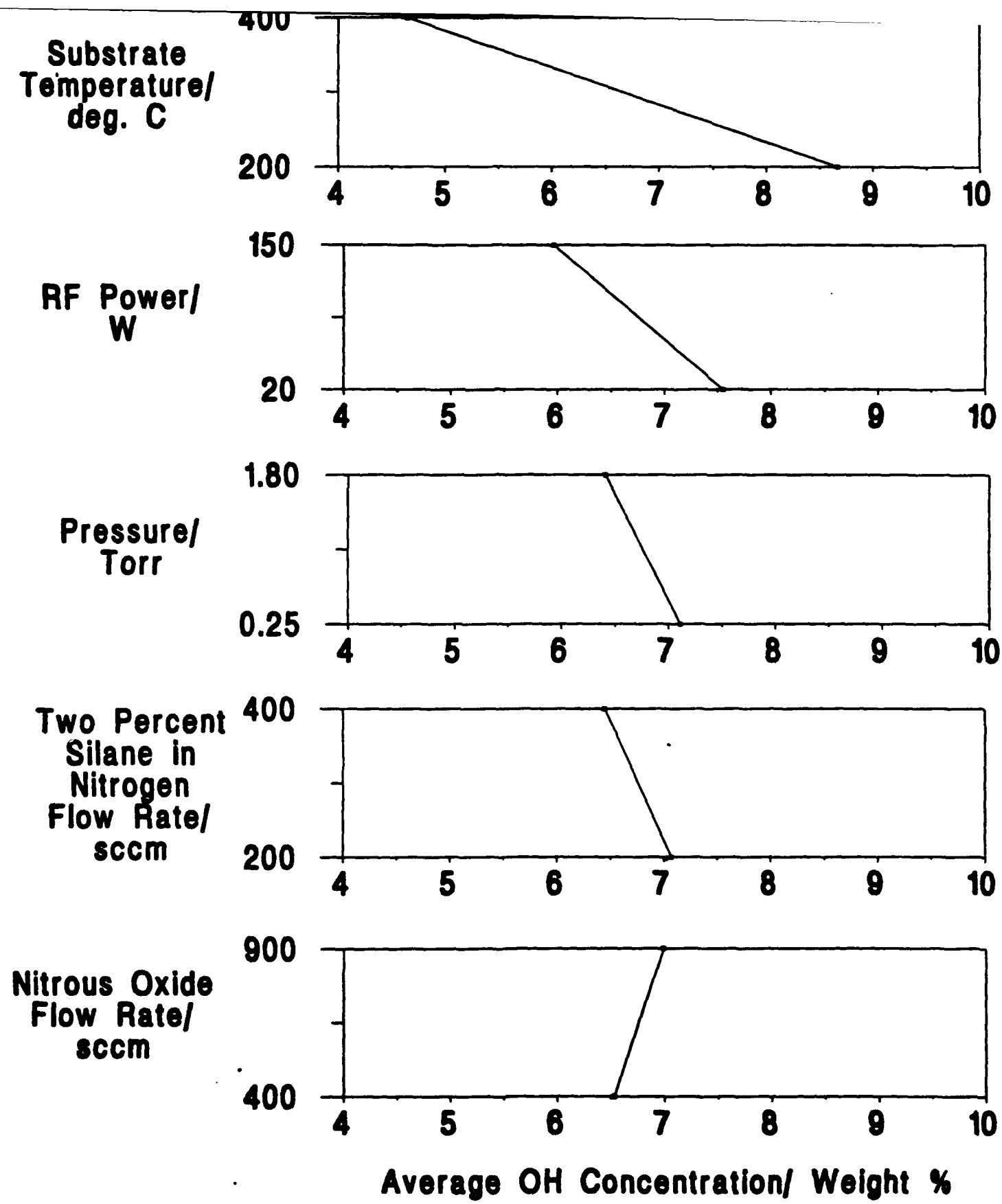

Figure 5.1-1. The effects of the deposition parameters on the silanol and water concentration (weight %).

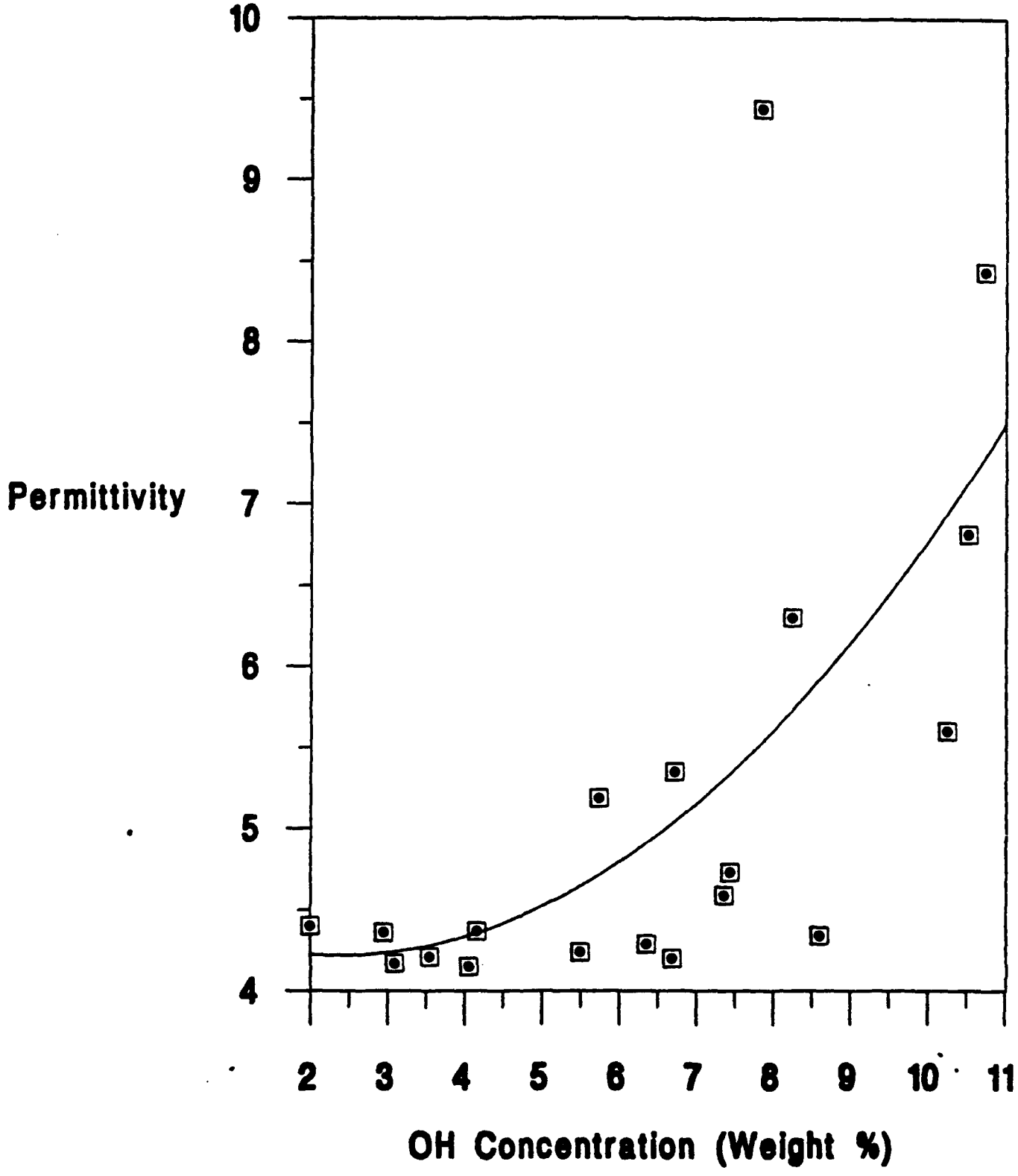

Figure 5.1-2. Silanol and water concentration (weight %) vs. permittivity.

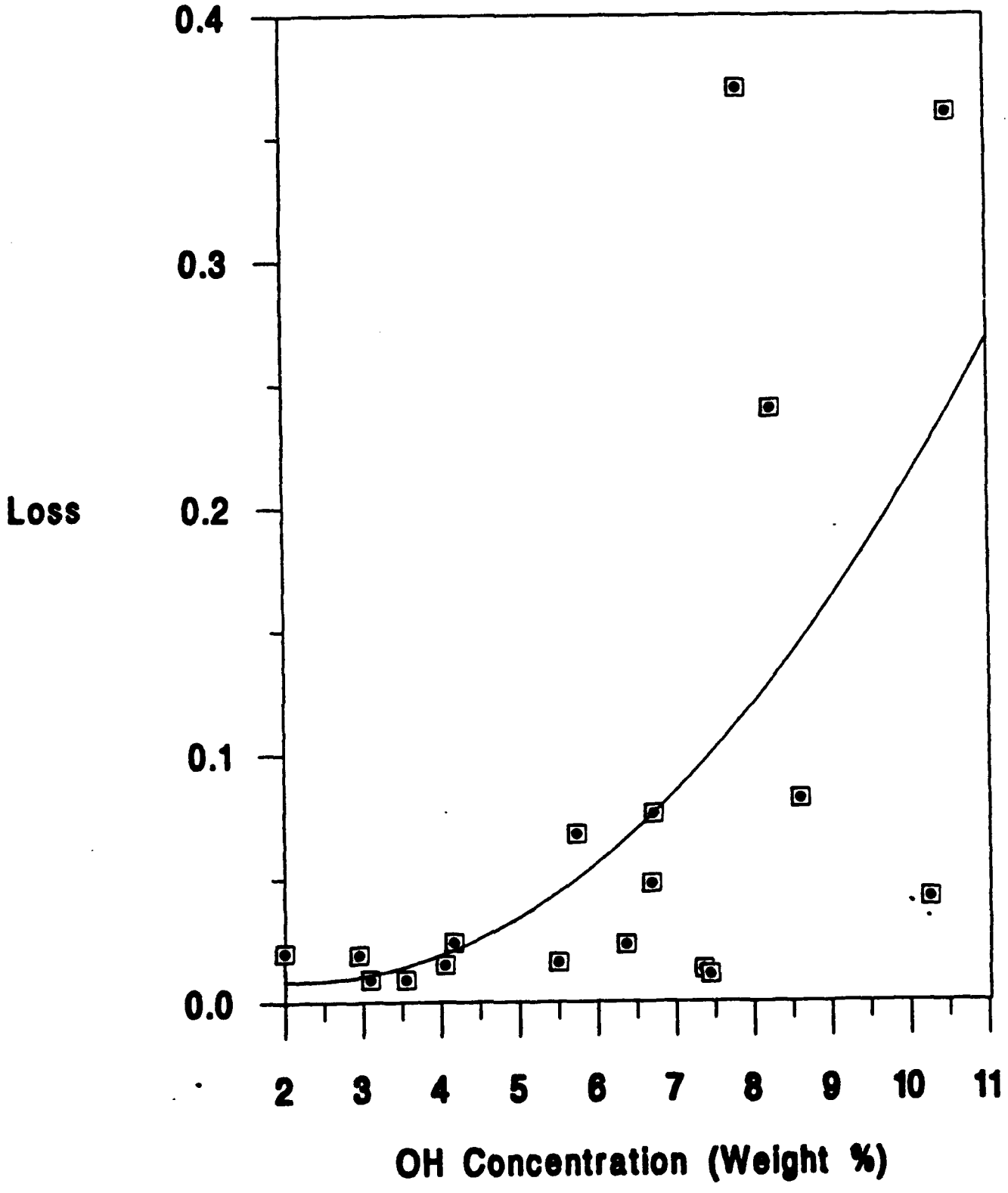

Figure 5.1-3. Silanol and water concentration (weight %) vs. loss.

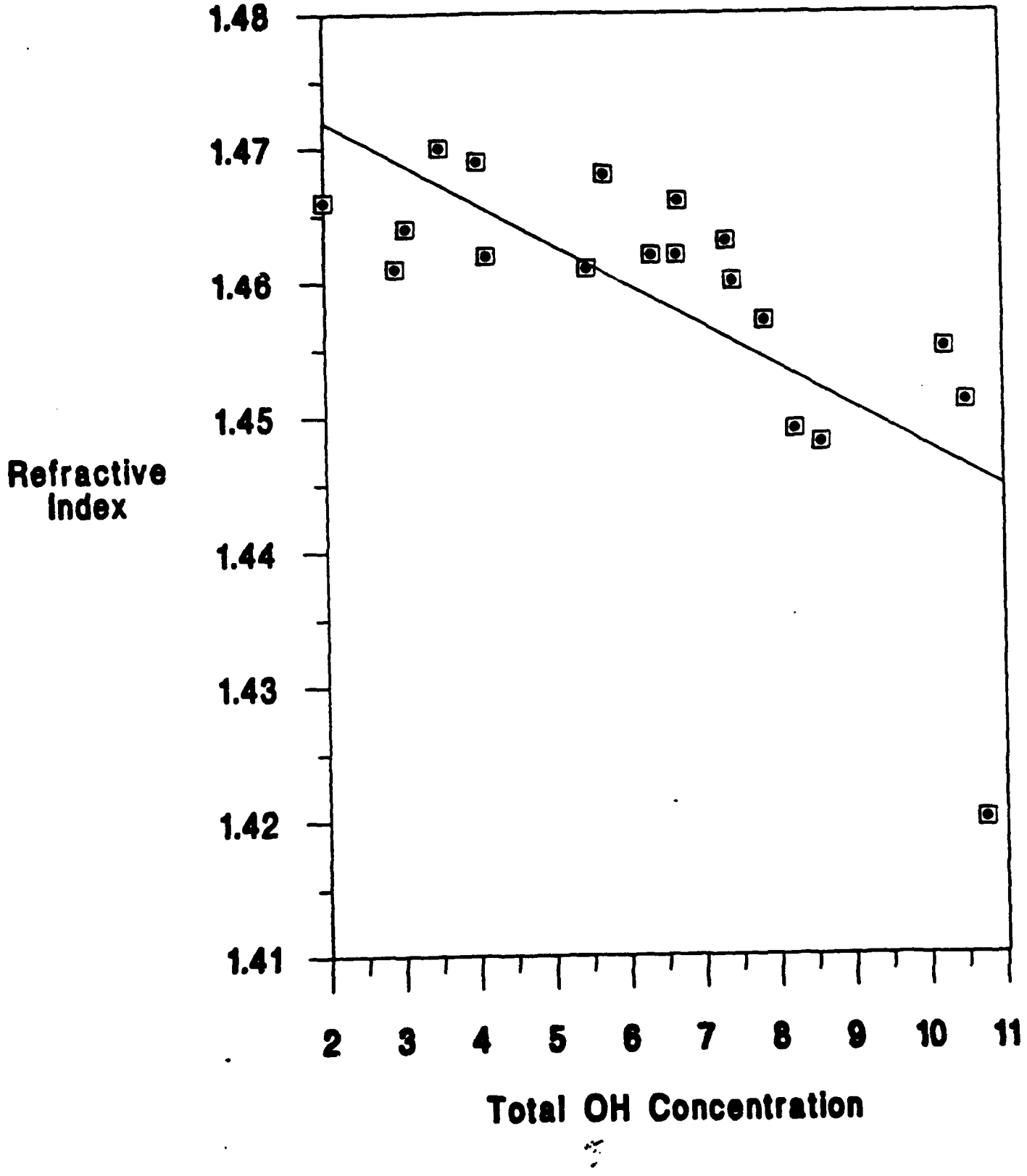

Figure 5.1-4. Silanol and water concentration (weight %) vs. refractive index.

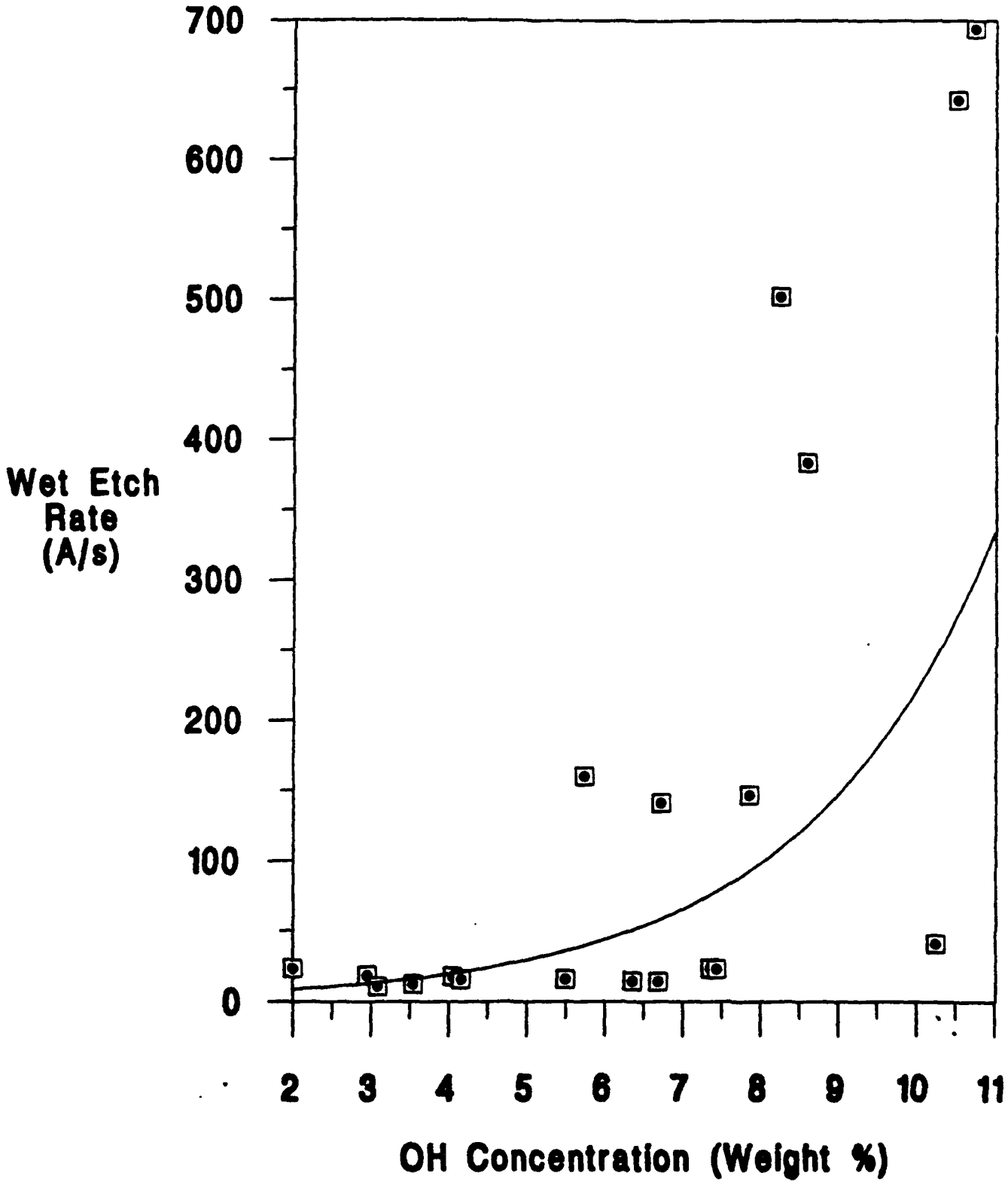

Figure 5.1-5. Silanol and water concentration (weight %) vs. wet etch rate (Å/s).

5.2 Porous Silica Dielectric Layers

Purpose

Porous silica is potentially a very attractive dielectric materials for MCMs because it is (1) very low dielectric constant (i.e. 1.8) by virtue of its porosity, (2) relatively high thermal conductivity, about the same as polymeric systems, and (3) potentially very low cost.

Based on these very attractive attributes, we have investigated the formation of porous silica via sol-gel processing. Thin film sol-gel films have not been demonstrated. The technical objectives include producing strong materials without the high temperature firing used in bulk materials, and to extract the residual salts in a reasonable time.

In summary, the formation of porous silica of suitable quality is very difficult, and at this time we do not see the fruition of this material.

Approach

Sol-gel processing starts with a potassium silicate solution and precipitates porous silicon dioxide. In bulk studies, high temperature firing of the deposited silica results in a very stable, hard materials. Sol-gel films were coated on glass and silicon test samples. The post deposition treatment included modest heat treatments and salt leaching steps. The figures of merit for the films were its dielectric constant at low and high frequency, and the mechanical integrity of the film.

Results

After a considerable effort adapting bulk porous silica processing to thin film technology, reasonably stable films were formed. The thickness was improved to over 10 mm, and the ionic impurity level was decreased. The effective DC dielectric constants of <10 were achieved, without consistent reproducibility. These values show considerable progress, however, the results fall significantly short of the objectives and work on this task has been terminated.

In general, the fabrication of porous dielectrics has several liabilities. In addition to the removal of by-products, the formation of pores in the dielectric flirts with a potentially significant yield loss. The production of pores while still

providing a sealed surface of adequate mechanical strength, can be a treacherous balance to achieve.

6. Electrical Characterization

The electrical measurements of the material dielectric properties are made using in-situ structures on the processed wafers. Two different sets of test structures have been used to date. The first test structures contained two sets of capacitors and microstrip transmission lines of various lengths. For the second generation wafers, several different in-situ test structures were considered and it was decided to use capacitors and microstrip resonators as the primary test structures.

Capacitors have the advantage that the complex impedance can be measured over a range of frequencies, thus values of the dielectric constant and loss can be obtained at each frequency. As frequencies increase, however, capacitors become distributed networks imposing an upper usable frequency limit. Larger capacitors, although having a lower frequency usable frequency limit, have the advantage of minimizing the effect of parasitic fringe capacitance and measure a larger area of dielectric material. The second generation test wafers thus had capacitors of different sizes.

Resonant structures offer an alternative method to measure the dielectric properties of materials and potentially provide more accurate loss data [6.1-1]. The reflection coefficient, S11, and the transmission coefficient, S21, of a resonator versus frequency have a set of nulls at the discrete resonant frequencies of the structure. The resonant frequency of the nulls and the frequency separation of adjacent nulls are functions of the dielectric constant of the substrate and the length of the resonator. Knowing the length of the resonator, the dielectric constant of the substrate can be determined. The depth of the null is determined by the metal loss and the dielectric loss. After the metal loss has been determined, the loss of the dielectric is calculated [6.1-2-6.1-4].

After considering a variety of resonator structures, it was decided to use the both the "T" resonator reported by Amey and Curilla [6.1-55] and an end-coupled half-wave resonator. The "T" resonator is a through line with a quarter-wave open circuited stub. The end-coupled resonator has lighter coupling and is a one-port. Both of these resonators are shown in Figure 6.1.

There are several compromises which must be accepted to fabricate these resonant structures on the processed wafers. The first is the very thin top metal layer (3 - 5 μm) which gives substantial metal loss. A second limitation is that it is difficult to lightly couple to the resonant line with a microstrip gap since the coupling gaps must be on the order of the dielectric thickness (5 - 7 μm). The small dielectric thickness requires a line width of approximately 9 microns to fabricate 50 ohm lines. It was decided to use a lower impedance line, Zo = 29 ohms which has a line width of approximately 25 microns. Since data can only be obtained at the discrete resonant frequencies, the resonant lines were made of two different lengths which are as long as possible (approximately 5 cm) to give the maximum number of nulls.

The high frequency measurements of the capacitors and resonators are made by probing the wafers with a Design Techniques microwave prober. An HP 8510 network analyzer is used to measure the complex impedance of the capacitors and S11 and S21 of the resonators versus frequency. The material dielectric constant, ε_r, and the loss tangent are calculated from the measured data using iterative methods and the microstrip models in the HP Microwave Design System software package. The actual probing of the wafers is manual but the collection and reduction of the experimental data is automated.

6.1 First Generation Test Wafer Measurements

The capacitances on the first generation wafers range from about 0.5 to 3.0 pF . Table 6.1-1 shows dielectric constant and loss tangent data from first generation polyimide wafers (lots 10, 11, and 12). The nominal low frequency dielectric constants for these wafers are 3.5, 3.3, and 3.0 respectively. The measured values of dielectric constant are reasonable, however, the loss tangents are higher than expected.

After examining the results from the first generation wafers, it was decided to make larger capacitors on the second generation wafers to minimize fringing capacitance effects and circular instead of rectangular to make fringe capacitance correction easier.

6.2 Second Generation Wafer Measurements

To date, approximately 24 lots have been produced using the second generation mask. Data from the larger capacitors have not been useful, but the T-

resonators have proved successful. The end coupled resonators appear to have very low coupling, making it difficult to determine resonant frequencies.

Dielectric constant data seems quite reasonable in most cases; However, loss tangent results are not very reliable. Table 6.1-2 shows some representative results for several types of polymers. Notice that the values of the relative dielectric constant generally only change 2 or 3 percent over the frequency range from 1 to 9 GHz, and are generally quite close to the nominal relative dielectric constant. These results are much better than the first generation results which varied by tens of percentage points over the frequency range. The loss tangent data for the second generation wafers is also usually much lower than the loss tangents calculated from the first generation wafers. However, even using the resonators and the more complicated computer models, the loss tangent still varies much more than would be expected.

In an effort to help explain the wide variations being seen in the loss tangent results, a set of simulations were run in order to determine the sensitivity of the relative dielectric constant and loss tangent to the various physical parameters of the resonator. Five T-resonator parameters were considered (resonator length, micrstrip width, dielectric thickness, metal thickness, and metal conductivity). Each of these parameters was changed slightly from a reference, one parameter change per simulation, and the change in relative dielectric constant and loss tangent was calculated. The results are summarized in Table 6.1-3. The simulations indicated that the relative dielectric constant was relatively insensitive to each parameter except the length of the resonator. The loss tangent however was extremely sensitive to all the physical characteristics. This is mainly due to the fact that the metal causes most of the loss in the resonator.

Future efforts will include further refinement of the measurement technique and models used in calculations.

Table 6.1-1: Dielectric Constant and Loss Results from First Generation Wafers

Freq.	Lot 10 (ε_r = 3.5)		Lot 11 (ε_r = 3.3)		Lot 12 (ε_r = 3.0)	
(GHz)	ε_r	Loss Tan	ε_r	Loss Tan	ε_r	Loss Tan
0.05	3.64	0.02	3.84	0.02	3.09	0.02
0.5	3.51	0.01	3.67	0.01	2.98	0.01
1.00	3.50	0.01	3.66	0.01	2.98	0.01
2.50	3.46	0.02	3.62	0.02	2.95	0.03
5.00	3.41	0.04	3.58	0.04	2.93	0.06
10.00	3.32	0.04	3.49	0.04	2.90	0.09
18.00	3.10	0.04	3.32	0.05	2.84	0.17

Table 6.1-2: Dielectric Constant and Loss Results from Second Generation Wafers

Res. Freq.	BCB (ε_r = 2.7)		Lot 12 (ε_r = 3.0)		PD2732 (ε_r =)	
(GHz)	ε_r	Loss Tan	ε_r	Loss Tan	ε_r	Loss Tan
2.50	2.67	0.002	2.97	0.000	3.54	0.046
4.25	2.74	0.006	3.02	0.005	3.58	0.034
6.00	2.73	0.010	3.02	0.002	3.50	0.025
8.00	2.72	0.027	2.99	0.054	3.49	0.023

Table 6.1-3: Dielectric Constant and Loss Tangent Sensitivity to Physical Parameters

Change in Physical Parameters	Max. Change in ε_r	Max. Change in Loss Tan
Length (1%)	2.33%	200%
Width (5%)	0.67%	700%
Dielectric Thickness (5%)	1.67%	440%
Metal Thickness (5%)	0.00%	300%
Conductivity (5%)	0.67%	420%

7. Cost Analysis

The major draw back to gold metallization for MCMs has been the materials cost associated with the gold itself. A cost analysis of these MCM structures demonstrates that noble metal MCMs can actually be manufactured at lower costs than some copper processes. Because there are numerous alternatives in the fabrication of copper MCMs, a simple generic comparison will be made for the purpose of this discussion.

Today, high density MCMs cost targets are about $20/sq. in. with a near term goal of $10/sq. in. Using conservative estimates, the metal cost for a typical 4 metal-layered structure using gold is about $1/sq. in. This is based on a $330/oz. cost of bulk gold, a 20% purification cost, and 2.2 sq. in. of gold metal per sq. in. of MCM at a thickness of 3.0 mm. That is, each metal layer is approximately 3.0 mm thick, and the sum of the areas of the power, ground, and 2 signal layers is 2.2 times the gross area of the MCM. Allowing for a more aggressive estimation with respect to purification costs and metal usage, one could feasibly estimate the metal cost for a similar structure as low as $0.50/sq. in. Thus, the cost of the gold adds only about 2.5 - 5% of the total MCM cost based on the overall target of $20/sq. in.

The cost of the insulator can be an even greater expense than that of the metallization. For example, the cost of a spin-coated organic insulator in Table 1 can range from $250 to over $2000 per liter ($0.60 to $2.50/sq. in. for the 4-layer MCM assuming a 5 mm thickness and 80% loss during spin-on). In comparison, 4 layers of silicon dioxide can be deposited at approximately $0.30/sq. in. In any case, the cost of the dielectric layers will be equal for any MCM metallization process, and for further calculations a value of $1/sq. in. will be assumed. Similar estimates can be performed to show that substrate costs will range from $0.60 to $1/sq. in., assuming the use of either 100 or 200 mm diameter silicon wafers.

This means that just the fabrication cost for each square inch of a 4-layered structure (total minus materials) will cost $16 to $18, based on a total cost of $20/sq. in., and assuming the costs of the gold metal, dielectric material, and substrate are all approximately $1/sq. in. Thus, approximately 80-90 % of the cost of an MCM will stem from fabrication costs (processing, equipment, labor, etc.). If the cost of labor, equipment, and secondary materials is the same for

each layer (4 layers of metal, 4 layers of insulator), then the cost of each layer is about $2/sq. in.

In copper or aluminum structures, a final bond pad layer is added in order to terminate the structure with a bondable metal (i.e. gold). If a gold metallization process is used throughout the fabrication, however, the final bond pad layer is no longer necessary. This eliminates one whole layer and saves approximately $2/sq. in. in processing costs. Thus, in the elimination of just one processing step through gold metallization, twice the cost of all the gold in the entire structure can be saved.

There are additional advantages of gold processing over copper. Several of the polyimide formulations presently used for the dielectric layers contain polyamic acid which can attack metals such as copper [16]. Added concerns are raised when hygroscopic materials are in use because the 2-4% water content, common in polyimides, can cause corrosion of copper lines. To reduce this corrosion and to promote adhesion between the metal and polyimide, many MCM fabricators deposit a 1000-10,000 Å layer of a barrier metal such as titanium, nickel, or chromium on all exposed surfaces of the copper or aluminum. This process sometimes involves the electroless deposition of metals, such as nickel or chromium, which adds at least four processing steps to the original eight steps already required for each metal layer, or approximately 25% additional labor and materials. In other cases the copper is lithography patterned with a barrier metal, adding somewhat more than four processing steps per metal layer. These corrosion protection layers degrade the quality of the copper metal, and therefore the conductivity, and can greatly magnify the "skin effect" phenomenon seen above the gigahertz threshold. Additionally, the methods employed to attain a corrosion protection layer are often plagued by high defect densities and unreliability.

As additional processing steps are added for bonding or for corrosion protection of the copper, the yield can be dramatically affected. The yield of an MCM fabrication process can be described using a clustered defect model,

$$Y_i = \left(1 + {}^{AD_o}/_{\alpha}\right)^{-\alpha}$$

where Y_i is the yield of any process step, A is the area on the MCM susceptible to the defect, D_o is the defect density, and α is the defect cluster parameter (usually

-1). If the overall yield is simply the product of the yield from each step, Y_i, then the overall yield will suffer tremendously as the area of the MCM increases. With a 25% increase in the number of processing steps, the cost of the MCM will increase alarmingly, as both the increased processing costs and decreased yields must be accounted for. For instance, assuming a yield of 90% from each processing step, a fabrication process for gold consisting of 28 steps would give a total yield of 24%. A similar copper process consisting of 32 steps (a minimal increase of 4 steps over gold) would have a total yield of 19%, 5% lower than the gold process. Thus, the yield for the copper process would be 20% less than that for the gold process. Notice that even a processing step yield of 90% would require a defect density of 0.03 for a 4 sq. in. structure. Lower yields on individual processing steps would only magnify the difference in overall yields between copper and gold processes. It is difficult to quantify this yield advantage in monetary terms, but it fair to say that the yield of a gold metallization process will be substantially better than any comparable copper processes. Yield considerations alone are the dominant driving force towards gold metallization of MCMs over current copper and aluminum processes.

8. Students and Tasks

Anne Sullivan

Advising Began: Winter 1990
Comprehensive Examination Passed: Summer 1991
Graduation Date: Spring 1995
Thesis Title: The Auto-catlaytic Deposition of Gold

Thomas Hodge

Advising Began: Winter 1990
Comprehensive Examination Passed: Summer 1991
Graduation Date: Spring 1995
Thesis Title: Microstructures for Measuring Mechanical and Thermal Properties of Thin Polymer Structures.

Martin Ceiler

Advising Began: Fall 1991
Graduation Date: Fall 1993
Thesis Title: Inorganic Dielectrics for GHz Multi-Chip Modules

Bilal Sinno

Advising Began: Fall 1991
Graduation Date: Fall 1993
Thesis Title: Properties of Polyquinoline Interlevel Dielectrics

Kirk Laursen

Advising Began: Fall 1991
Comprehensive Examination Passed:
Graduation Date: Spring 1996
Thesis Title: High FrequencyProperties of Low Dielectric Constant Insulators

Geneva Tatem

Advising Began: Winter 1993
Comprehensive Examination Passed:
Graduation Date: Summer 1997
Thesis Title: Electromigration and Moisture Studies for High Frequency Multi-chip Modules

Undergraduate Students

Joel Edwards, Winter 1991 - Winter 1992, "DC Magnetron Sputtering"

Michael Houston, Winter 1991 - Spring 1993, "Photolithography and electron microscopy"

Mahesh Thadhani, Winter 1991 - Winter 1992, "Electrodeposition of Gold"

Gareth Sampson, Winter 1991 - Spring 1992, "Reactive Ion Etching"

Todd Cloud, Spring 1991 - Present, " Photosensitive Polyimides"

Ralph Redd, Fall 1991 - Spring 1993, "Semiconductor Metallization"

Cassondra Farmer, Summer 1992 - Spring 1993, "Wafer Coating Using MTI Flexifab"

Barry Coe, Summer 1992 - Fall 1992, "Electroplating of Gold"

Guerry Taylor, Summer 1992 - Present, "Reactive Ion Etching"

George Obath, Winter 1993 - Spring 1993, "Electroplating"

Christine Roberts, Fall 1992 - Spring 1993, "Chemical Etching"

Carnley Norman, Winter 1993 - Present, "Reactive Ion Etching

9. Publications and Presentations

Vogt, K., Kohl, P.A., Bell, R., Bottomley, L.A., and Carter, B., "Characterization of Thin Titanium Oxide Adhesion Layers on Gold: Resistivity, Morphology, and Composition.", Surface Science, in-press.

Cloud, T., Houston, M., Kohl, P.A., and Bidstrup, S.A., "High Performance Noble Metal MCMs" IEEE Transactions on Manufacturing Systems., Submitted.

Hodge, T., Landmann, B., Kohl, P.A., and Bidstrup, S.A., "Rapid Thermal Curing of Polymer Interlayer Dielectrics" Journal of Microcircuits & Electronic Packaging

Hodge, T., Ceiler, M., Sinno, B., Kohl, P.A., Bidstrup, S.A., Hertling, D.R., "Materials and Processes for High Performance MCMs" IEPC, September 1993.

Hertling, D.R., Laursen, K., Bidstrup, S.A., Kohl, P.A., Arroz, G.S.., "Measurement of the Electrical Properties of High Performance , Low Cost Dielectric Materials for Multichip Modules." IEPC, September 1993.

Hodge, T., Bidstrup, S.A., and Kohl, P.A., "The Effect of Moisture and Temperature on the Dielectric Properties of Polyimides", The Electrochemical Society, October, 1992.

Han, S.S., Ceiler, M., Bidstrup, S.A., May, G., and Kohl, P.A., "Neural Network-Based Modeling of the Plasma-Enhanced Chemical Vapor Deposition of Silicon Dioxide", IEEE/CHMT International Electronics Manufacturing Technology Symposium, 1993.

Frye, D.C., Harris, R.H., Heistrand, R.H., Moyer, E.S., Rutter, E.W., Garrou, P., Berry, M.J., Rogers, B., Turlik, I., Bidstrup, S.A., Hodge, T., Kohl, P.A., Taylor, G., Berry, K., David, F., and Lanka, M., "Via Generation in Cytclotene", VLSI Packaging, Kyoto, Japan December 2, 1992.

10. References

[3.1-1] A. Scorzoni, B. Neri, C. Caprile, F. Fantini, Materials Science Reports, **7** (1991).

[4.1-1] D. Boese, S. Herminghaus, D. Y. Yoon, J. D. Swalen and J. F. Roberts, "Stiff Polyimides: Chain Orientation and Anisotropy of the Optical and Dielectric Properties of Thin Films", MRS Symposium Proceeding, p. 379-386, Vol. 227 (1991).

[4.3-1] G. MacBeth, "Prebaking Positive Photoresists", *Proc. Kodak Microelectronics Seminar Interface '82*, San Diego, CA, pp. 87-92 (1983).

[4.3-2] J.T. Pan and I. Blech, *Journal of Applied Physics*, **55** (8), pp. 2874-2880 (1984).

[4.3-3] A.C. Adams, D.P. Schinke, and C.D. Capio, *Journal of the Electrochemical Society: Solid State Science and Technology*, **126**, pp. 1539-1543 (1979).

[4.3-4] N. Takahashi, D.Y. Yoon, and W. Parrish, "Molecular Order in Condensed States of Semiflexible Poly(Amic Acid) and Polyimide", *Macromolecules*, **17**. pp. 2583-2588 (1984).

[4.3-5] H. Ishida, S.T. Wellinghoff, E. Baer, and J.L. Koenig, "Spectroscopic Studies of Poly[N,N'-bis(phenoxyphenyl)pyromellitimide]. 1. Structures of the Polyimide and Three Model Compounds", *Macromolecules*,**13**, pp. 826-834 (1980).

[4.3-6] J.C. Coburn and M.T. Pottinger, "The Influence of Processing Conditions on Structure, Properties and Stress Development in Spin Coated Polyimide Films", *Proceedings of Advances in Polyimide Science and Technology*, Ellenville, NY, p. 360-374 (1991).

[4.3-7] Benzocyclobutene Polymer Data Sheets, Dow Chemical Co., Microelectronic Polymers Division, Midland, MI.

[4.3-8] R.H. Heistand , R. DeVellis, T.A. Manial, A.P. Kennedy, T.M. Stokich, P.H. Townsend, P.E. Garrou, T. Takahashi, G.M. Adema, M.J. Berry, and I. Turlik, "Advances in MCM Fabrication with Benzocyclobutene (BCB) Dielectric", *International Journal of Microcircuits and Electronic Packaging*, **15**, No. 4, pp. 183-194 (1992).

[4.3-9] D.C. Frye, R.F. Harris, R.H. Heistand II, E.S. Moyer, E.W. Rutter, P. Garrou, M.J. Berry, B. Rogers, I. Turlik, S. Bidstrup, T. Hodge, P. Kohl, G. Taylor, K. Berry, F. David, and M. Lanka, "Via Generation in Cyclotene", presented at VLSI Packaging Workshop, Kyoto, Japan, Dec. 2, 1992.

[5.1-1] J.D. Chapple-Sokol, W.A. Pliskin, R.A.Conti, E. Tierney, and J. Batey, J. Electrochem. Soc., 138, 12, 3723 , (1991).

[5.1-2] H.P.W. Hey, B.G. Sluijk, and D.G. Hemmes, Solid State Technology, 33, 4, 139, (1990).

[5.1-3] P.C. Pai, S.S. Chao, Y. Takagi, and G. Lucovsky, J. Vac. Sci. Technol. A, 4, 3, 689, (1986).

[5.1-4] A.C. Adams, F.B. Alexander, C.D. Capio, and T.E. Smith, J. Electrochem. Soc., 128, 7, 1545, (1981).

[6.1] R. E. Collin, "Foundations for Microwave Engineering, Second Edition", McGraw-Hill Inc., 1992.

[6.2] L. N. Dworsky, "Modern Transmission Line Theory and Applications", Wiley, 1979.

[6.3] H. A. Wheeler, "Transmission-Line Properties of a Strip on a Dielectric Sheet on a Plane", IEEE Trans. Microwave Theory Tech., Vol. MTT-25, N. 8, 631-641, August 1977.

[6.4] R. A. Pucel, D. J. Masse and C. P. Hartwig, "Losses in Microstrips", IEEE Trans. Microwave Theory Tech., Bol. MTT-16, N. 6, 1064, June, 1968 and "Correction to Losses in Microstrips", IEEE Trans. Microwave Theory Tech., vol MTT-16, N. 12, pp 1064, December 1968.

[6.5] D. I. Amey and J. P. Curilla, "Microwave Properties of Ceramic Materials," 41st ETSC, May 1991.